Research Square

Preprints are preliminary reports that have not undergone peer review.
They should not be considered conclusive, used to inform clinical practice,
or referenced by the media as validated information.

Frequency-Energy Plots of Bistable Nonlinear Energy Sink

Mohammed Ameen Al Shudeifat (mohd.shudeifat@ku.ac.ae)
Khalifa University of Science Technology https://orcid.org/0000-0002-7973-2559
Adnan Salem Saeed
Khalifa University of Science Technology - Abu Dhabi Campus: Khalifa University of Science and Technology

Research Article

Keywords: Nonlinear Energy sink, nonlinear normal modes, frequency energy plot, bistable nonlinear energy sink

Posted Date: March 16th, 2021

DOI: https://doi.org/10.21203/rs.3.rs-197669/v1

License: This work is licensed under a Creative Commons Attribution 4.0 International License.
Read Full License

Version of Record: A version of this preprint was published at Nonlinear Dynamics on August 17th, 2021. See the published version at https://doi.org/10.1007/s11071-021-06802-8.

Frequency-Energy Plots of Bistable Nonlinear Energy Sink

Mohammad A. AL-Shudeifat

Aerospace Engineering, Khalifa University of Science and Technology,

Abu Dhabi,127788, UAE, mohd.shudeifat@ku.ac.ae

Adnan S. Saeed

Aerospace Engineering, Khalifa University of Science and Technology,

Abu Dhabi,127788, UAE, adnan.saeed@ku.ac.ae

Abstract

The nonlinear energy sink (NES), which is proven to perform rapid and passive targeted energy transfer (TET), has been has been employed for vibration mitigation in many primary small- and large-scale structures. Recently, the feature of bistability, in which two nontrivial stable equilibria and one trivial unstable equilibrium exist, is utilized for passive TET in what is known as Bistable NES (BNES). The BNES generates a nonlinear force that incorporates negative linear and multiple positive or negative nonlinear stiffness components. In this paper, the BNES is coupled to a linear oscillator (LO) where the dynamic behavior of the resulting LO-BNES system is studied through frequency-energy plots (FEPs), which are generated by analytical approximation using the complexification-averaging method and by numerical continuation techniques. The effect of the length and stiffness of the transverse coupling springs is found to affect the stability and topology of the branches and indicates the importance of the exact physical realization of the system. The rich nonlinear dynamical behavior of the LO-BNES system is also highlighted through the appearance of multiple symmetrical and unsymmetrical in- and out of- phase backbone branches, especially at low energy levels. The wavelet transform is imposed into the FEP for variety of initial conditions and damping content and it is found that the FEP has backbone branches at low energy levels associated with the oscillation of the bistable attachments about one of its stable equilibrium positions where passage through the unstable equilibrium position does not occur.

***Keywords**: Nonlinear Energy sink, nonlinear normal modes, frequency energy plot, bistable nonlinear energy sink.*

Introduction

The nonlinear energy sink (NES) is a light-weight nonlinear dynamical oscillator that employs an essentially nonlinear coupling element to engage in optimum passive TET from an associated primary structure to be localized or

dissipated by the NES. Due to single or cascade of resonance captures, the NES can perform rapid, passive, and nearly irreversible TET in a broadband frequency-energy fashion. The essentially non-linearizable coupling element significantly alters the global dynamics of the integrated system resulting in nonlinear interactions between structural modes. This causes passive energy exchange, a phenomenon that is not possible in linear dynamical absorbers except in the case of carefully tuned frequencies. Consequently, the NES has been intensively studied in literature for shock and seismic mitigation purposes to rapidly dissipate a significant portion of the energy induced into a structure.

Generally, the NESs can be categorized into translational and rotational depending on the nature of their motion. The basic element of the traditional translational NES employs a purely non-negative cubic restoring stiffness which is realized by transversely coupled linear springs in Type I NES. A variety of subtypes branch out from this nonlinear coupling method based on the nature of the coupling damping element, the characteristics of the nonlinear force or the number of nonlinearly attached masses [1–9]. Other types of translational NESs include the magnetic NES which is realized by a nonlinear magnetic force [10 – 12] and the vibro-impact NES which is realized by non-smooth nonlinearities imposed via impact surfaces to an otherwise linear tuned mass damper [1,13–21]. The other category, the rotational NESs, is realized by inertial coupling between the NES mass and the primary structure by means of a rigid rotating arm to generate a strongly nonlinear coupling force [22–27]. Additional research works have investigated using an oscillating arm or incorporating non-smooth nonlinearities to the rotational NESs attempting to enhance the irreversible nonlinear energy transfers [28,29]. Numerous research works show that both categories and many subtypes of the NESs yield enhanced “utilization” of the inherent structural

dynamics towards more effective response mitigation, without the necessity of adding more damping.

Recently, the idea of introducing the feature of bistability in which the NES possesses two nontrivial stable equilibria and one trivial unstable equilibrium has been addressed in [30-42]. A detailed numerical and analytical study of the bistable NES (BNES) having combined negative linear stiffness and positive cubic nonlinear stiffness terms shows that this type of NESs can achieve efficient TET for impulsively excited structures [30,31]. Following the analytical study in [30], it is found that the mechanisms leading to the energy exchanges between a low-energy impulsively excited linear oscillator and the BNES are a periodic alternating in-well and cross-well oscillations of the BNES and secondary nonlinear beats occurring when the dynamics evolves solely in-well [31]. In addition, the physical realization of the BNES is addressed in [32,33] where the nonlinearity is obtained by transverse linear springs that are compressed in their vertical position. Using Taylor-expansions, the generated nonlinear force incorporates negative linear and multiple positive or negative nonlinear terms. This resulted in a unique representation of the nonlinear force as it encloses up to seventh order nonlinear stiffness terms as opposed to cubic nonlinear terms only in most other works in literature. The resulting system is highly efficient compared to other existing NESs in literature for a wide range of initial impulsive energies [32]. The efficiency of the BNES is further analyzed using slow invariant manifold, asymptotic analysis and Melnikov analysis to predict the response regimes and their thresholds levels [34]. To optimize the performance of the BNES, a design criterion with a corresponding parameter is proposed in [34] and a novel tuning method using Lyapunov exponents is proposed in [35] which allows the BNES to avoid chaotic behavior and enhances TET. The BNES has also been employed to coupled linear

symmetrical oscillators with ungrounded configuration in [36] and with bistable grounding in [37]. In both cases, the capability of the BNES to achieve highly efficient TET is demonstrated. Given this high performance, the BNES was applied to cantilever beams [38], rotor systems [39,40], and pipes conveying fluids [41] for vibration suppression and incorporated with magnetic effects for structural seismic control [42].

The underlying nonlinear dynamical behavior has been revealed for some types of NESs based on studying frequency-energy dependences of Hamiltonian versions of linear systems attached to NESs. Therefore, frequency-energy plots (FEPs) have been generated via numerical and analytical methods. The FEPs of Hamiltonian versions of linear systems attached to NESs with odd-power stiffness coupling have been generated in several publications using analytical and numerical methods [1–5,43–48]. Similarly, FEPs of linear systems attached to rotating NES were obtained in [22,23] and systems attached to vibro-impact and piecewise NESs in [49–53]. In these sets of publications, fundamental backbone curves of 1:1 in-phase and antiphase resonances were obtained. In addition, several bifurcated subharmonic branches from fundamental backbones were also generated. The damped dynamics of considered systems have been studied by imposing wavelet-transform frequency spectra on the obtained FEPs. Accordingly, the NES nonlinear action of rapid energy transfer has been found to take place through single and cascade of resonance captures between the NESs and the associated linear structures responses. These studies has sufficiently revealed the underlying Hamiltonian and damped dynamics of aforementioned NESs.

In another set of publications [54,55] the damped dynamics of the NES itself has been studied. Therefore, formulas of displacement, velocity, frequency and energy decay curves have been obtained for odd-power stiffness NES. Based on

these formulas, a new formula for the relationship between displacement and velocity damping contents has been introduced in [54]. In [56], a method for generating plots of frequency versus nonlinear energy content (FNLPs) was introduced and directly applied into equations of motion where numerical simulation is not required *a priori*. This proposed method was employed later in [57] to reveal the underlying nonlinear dynamical behavior of modal damping content of some linear systems attached to NES.

In this paper, we discuss the BNES which is based on geometric nonlinearity that is realized by transversely coupled linear springs which are neither compressed nor elongated at two stable equilibrium positions. At the point where the linear springs are vertically aligned, an unstable equilibrium exists at which both linear springs have pre-stored potential energy. We consider a BNES attached to a linear oscillator (LO) where the resulting nonlinear coupling force consists of several negative and nonnegative linear and nonlinear stiffness components. We focus in particular on the frequency-energy plot (FEP) which is a representation of the nonlinear normal modes (NNMs) depicting the frequency content of the system with the corresponding energies. Accordingly, the dynamic behavior of the proposed BNES is investigated here on a FEP generated analytically using complexification averaging technique (CX–A) as well as via numerical continuation methods [58] of the undamped LO–BNES system to obtain the fundamental backbone branches of the nonlinear normal modes (NNMs). Consequently, the damped dynamics of the considered system is analyzed by imposing the wavelet transform of the obtained response into the obtained FEP.

System Description and Governing Equations

In the BNES, negative stiffness components appear when the transverse spring are neither compressed nor elongated at their stable equilibrium positions as shown in Fig. 1a. In this configuration both springs have presorted potential energy at zero displacements of the NES and the linear oscillator (LO) masses which in turn generates negative stiffness components. Accordingly, The BNES has two stable equilibrium positions at the NES relative displacement with LO $z = \pm z_c$ for $z_c > 0$ as shown in the figure. At $z = \pm z_c$ both springs are neither compressed nor elongated at their original physical length L. Furthermore, the BNES is unstable at $z = 0$. According to [32], the nonlinear restoring force of the springs can be approximated by the Taylor series expansion as

$$F_{nl} \cong \tilde{F}_{nl} = -2k\left(1-\frac{L}{L_0}\right)z - \frac{kL}{L_0^3}z^3 + \frac{3kL}{4L_0^5}z^5 - \frac{5kL}{8L_0^7}z^7 + O\left(z^9\right)$$

$$= k_1 z - k_2 z^3 + k_3 z^5 - k_4 z^7 + O\left(z^9\right), \qquad L_0 < L \tag{1}$$

where $k_1 = 2k\left(\frac{L}{L_0}-1\right)$, $k_2 = \frac{kL}{L_0^3}$, $k_3 = \frac{3kL}{4L_0^5}$ and $k_4 = \frac{5kL}{8L_0^7}$ for $L_0 < L$.

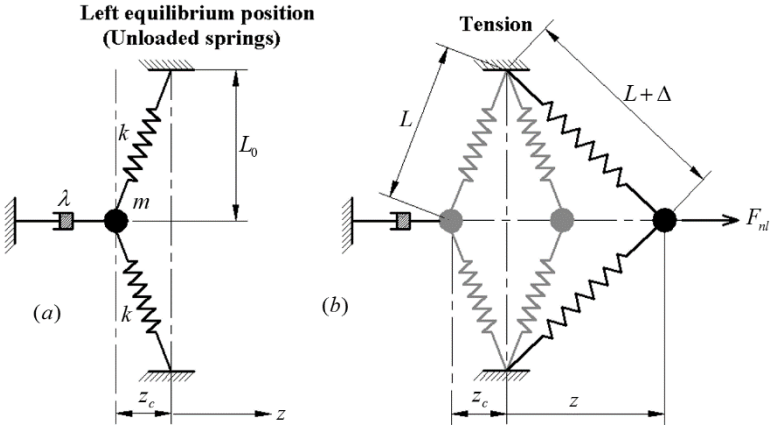

Fig 1 Physical configuration of the nonlinear damped oscillator.

The bistable nonlinear attachment in Fig. 1a of mass m is attached to the LO of mass M ($m << M$) as shown in Fig. 2. For $z_c > 0$, the equations of motions are written as

$$m\ddot{x}_1 + \lambda(\dot{x}_1 - \dot{x}_2) - k_1(x_1 - x_2) + k_2(x_1 - x_2)^3 - k_3(x_1 - x_2)^5 + k_4(x_1 - x_2)^7 = 0$$

$$M\ddot{x}_2 + \lambda_p\dot{x}_2 - \lambda(\dot{x}_1 - \dot{x}_2) + k_p x_2 + k_1(x_1 - x_2) - k_2(x_1 - x_2)^3 + k_3(x_1 - x_2)^5 - k_4(x_1 - x_2)^7 = 0 \quad (2)$$

where x_1 is the NES mass displacement, x_2 is LO mass displacement, λ is the damping of the NES attachment, λ_P is the damping of the linear structure and k_p is the stiffness of the linear structure. For $z_c = \sqrt{(L^2 - L_0^2)}$ and $z(0) = x_1(0) - x_2(0)$, the initial energy equation in the physical coordinates of the LO-BNES system is governed by

$$E_0 = \frac{1}{2}M\dot{x}_2(0)^2 + \frac{1}{2}m\dot{x}_1(0)^2 + \frac{1}{2}k_p x_2(0)^2 - \frac{1}{2}k_1 z(0)^2 + \frac{1}{4}k_2 z(0)^4 - \frac{1}{6}k_3 z(0)^6 + \frac{1}{8}k_4 z(0)^8 + \frac{1}{2}(2k)(L - L_0)^2 \quad (3)$$

It is clear from (3) that when $x_1(0) = x_2(0) = 0$ and $\dot{x}_1(0) = \dot{x}_2(0) = 0$, the initial presorted energy is obtained as $E_0 = k(L - L_0)^2$,

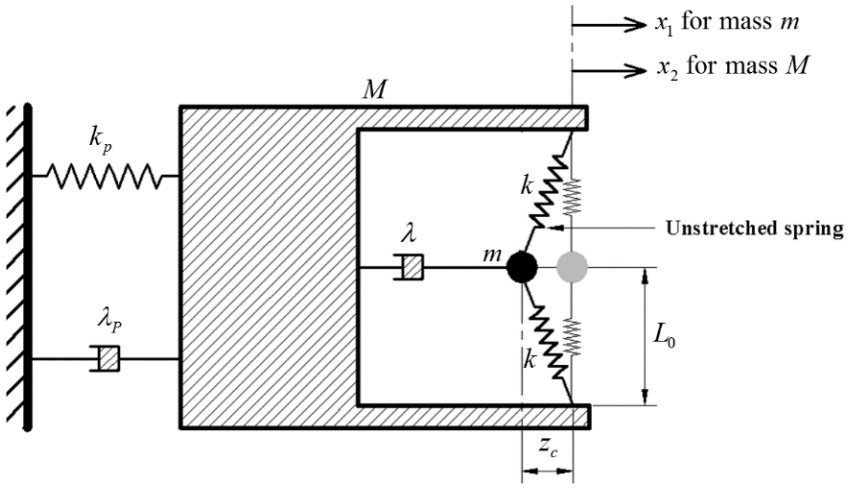

Fig 2 Single-degree-of freedom linear structure coupled to the modified NES.

FEP using Complexification Averaging Technique

To understand the dynamics of the LO-BNES system, we study the FEP of the system using complexification-averaging technique (CX–A) proposed by [58] through slow-fast partition of the dynamics to generate the backbone branches S11±; branches corresponding to motions where the LO and the BNES possess identical dominant frequency components.

Normalizing (2) with respect to the mass M gives

$$\varepsilon\ddot{x}_1 + \bar{\lambda}(\dot{x}_1 - \dot{x}_2) - \bar{k}_1(x_1 - x_2) + \bar{k}_2(x_1 - x_2)^3 - \bar{k}_3(x_1 - x_2)^5 + \bar{k}_4(x_1 - x_2)^7 = 0$$

$$\ddot{x}_2 + \bar{\lambda}_p\dot{x}_2 - \bar{\lambda}(\dot{x}_1 - \dot{x}_2) + \omega_0^2 x_2 + \bar{k}_1(x_1 - x_2) - \bar{k}_2(x_1 - x_2)^3 + \bar{k}_3(x_1 - x_2)^5 - \bar{k}_4(x_1 - x_2)^7 = 0 \quad (4)$$

where

$$\bar{\lambda}_p = \frac{\lambda_p}{M} \qquad \bar{\lambda} = \frac{\lambda}{M} \qquad \varepsilon = \frac{m}{M} \qquad \omega_0^2 = \frac{k_p}{M} \qquad \bar{k}_i = \frac{k_i}{M} \qquad i = 1,2,3,4$$

Assuming a conservative system (no damping dissipation effects: $\bar{\lambda}_p = \bar{\lambda} = 0$) and $\omega_0^2 = 1$, we perform the complexification of the dynamics, the first stage of the process, by introducing new complex variables given as:

$$\begin{aligned} \psi_1 &= \dot{x}_1 + j\omega x_1 \\ \psi_2 &= \dot{x}_2 + j\omega x_2 \end{aligned} \quad (5)$$

where ω is the dominant fast frequency of oscillation. Substituting (5) into (4) gives:

$$\varepsilon\left(\dot{\psi}_1 - \frac{j\omega}{2}(\psi_1 + \psi_1^*)\right) + j\bar{k}_1\left(\frac{\psi_1 - \psi_1^*}{2\omega} - \frac{\psi_2 - \psi_2^*}{2\omega}\right) - j\bar{k}_2\left(\frac{\psi_1 - \psi_1^*}{2\omega} - \frac{\psi_2 - \psi_2^*}{2\omega}\right)^3 + j\bar{k}_3\left(\frac{\psi_1 - \psi_1^*}{2\omega} - \frac{\psi_2 - \psi_2^*}{2\omega}\right)^5 - j\bar{k}_4\left(\frac{\psi_1 - \psi_1^*}{2\omega} - \frac{\psi_2 - \psi_2^*}{2\omega}\right)^7 = 0$$

$$\dot{\psi}_2 - \frac{j\omega}{2}(\psi_2 + \psi_2^*) - \frac{j(\psi_2 - \psi_2^*)}{2\omega} - j\bar{k}_1\left(\frac{\psi_1 - \psi_1^*}{2\omega} - \frac{\psi_2 - \psi_2^*}{2\omega}\right) + j\bar{k}_2\left(\frac{\psi_1 - \psi_1^*}{2\omega} - \frac{\psi_2 - \psi_2^*}{2\omega}\right)^3 - j\bar{k}_3\left(\frac{\psi_1 - \psi_1^*}{2\omega} - \frac{\psi_2 - \psi_2^*}{2\omega}\right)^5 + j\bar{k}_4\left(\frac{\psi_1 - \psi_1^*}{2\omega} - \frac{\psi_2 - \psi_2^*}{2\omega}\right)^7 = 0 \quad (6)$$

where $*$ indicates complex conjugates.

Given that we are interested in the periodic solutions (at fast frequency ω) where the LO and the BNES oscillate with the same fast frequency, we can express the complex variables defined in (5) in terms of fast oscillations of frequency ω, $e^{j\omega t}$, modulated by slowly varying complex amplitudes $\phi_i(t)$, $i = 1,2$:

$$\psi_1(t) = \phi_1(t)e^{j\omega t}$$
$$\psi_2(t) = \phi_2(t)e^{j\omega t} \quad (7)$$

Substituting (7) into (6) gives the following equations which are still exact representations of (4)

$$\varepsilon\left(\dot{\phi}_1 e^{j\omega t} + j\omega\phi_1 e^{j\omega t} - \frac{j\omega}{2}\left(\phi_1 e^{j\omega t} + \phi_1^* e^{-j\omega t}\right)\right) + j\bar{k}_1\left(\frac{\phi_1 e^{j\omega t} - \phi_1^* e^{-j\omega t} - \phi_2 e^{j\omega t} + \phi_2^* e^{-j\omega t}}{2\omega}\right) - j\bar{k}_2\left(\frac{\phi_1 e^{j\omega t} - \phi_1^* e^{-j\omega t} - \phi_2 e^{j\omega t} + \phi_2^* e^{-j\omega t}}{2\omega}\right)^3 + j\bar{k}_3\left(\frac{\phi_1 e^{j\omega t} - \phi_1^* e^{-j\omega t} - \phi_2 e^{j\omega t} + \phi_2^* e^{-j\omega t}}{2\omega}\right)^5 - j\bar{k}_4\left(\frac{\phi_1 e^{j\omega t} - \phi_1^* e^{-j\omega t} - \phi_2 e^{j\omega t} + \phi_2^* e^{-j\omega t}}{2\omega}\right)^7 = 0 \quad (8)$$

$$\dot{\phi}_2 e^{j\omega t} + j\omega\phi_2 e^{j\omega t} - \frac{j}{2\omega}\left(\phi_2 e^{j\omega t} - \phi_2^* e^{-j\omega t}\right) - \frac{j\omega}{2}\left(\phi_2 e^{j\omega t} + \phi_2^* e^{-j\omega t}\right) + \frac{\phi_1 e^{j\omega t} - \phi_1^* e^{-j\omega t}}{2j\omega} - j\bar{k}_1\left(\frac{\phi_1 e^{j\omega t} - \phi_1^* e^{-j\omega t} - \phi_2 e^{j\omega t} + \phi_2^* e^{-j\omega t}}{2\omega}\right) + j\bar{k}_2\left(\frac{\phi_1 e^{j\omega t} - \phi_1^* e^{-j\omega t} - \phi_2 e^{j\omega t} + \phi_2^* e^{-j\omega t}}{2\omega}\right)^3 - j\bar{k}_3\left(\frac{\phi_1 e^{j\omega t} - \phi_1^* e^{-j\omega t} - \phi_2 e^{j\omega t} + \phi_2^* e^{-j\omega t}}{2\omega}\right)^5 + j\bar{k}_4\left(\frac{\phi_1 e^{j\omega t} - \phi_1^* e^{-j\omega t} - \phi_2 e^{j\omega t} + \phi_2^* e^{-j\omega t}}{2\omega}\right)^7 = 0$$

The second step of the CX–A technique is the averaging of the equations in (8) with respect to the fast frequency ω. Therefore, only the terms containing the fast frequency are considered leading to a set of complex modulation equations constituting the approximate slow flow reduction of the dynamics. Following that, a set of polar representations given as

$$\phi_1 = Ae^{j\alpha}$$
$$\phi_2 = Be^{j\beta} \qquad (9)$$

are introduced where A, B are real amplitudes and α, β are real phases. After rearranging and using Euler's formula$e^{ix} = \cos(x) + j\sin(x)$, the real and imaginary parts of the resulting equations can be separately set to zero which represent the slow evolution of the real amplitudes and the phases of the modulation.

To impose stationary conditions on the modulation equations, the derivatives with respect to time are set to zero. Hence, the periodic solutions on the backbone branches can be computed. Considering the trivial solution by assuming identity of phases ($\alpha = \beta$), the resulting equations are solved (explicitly) using MATLAB to

obtain the values of amplitudes A and B for each considered frequencyω. Given that the conserved energy of the system can be expressed as

$$E = \frac{X^2}{2} - \bar{k}_1 \frac{(V-X)^2}{2} + \bar{k}_2 \frac{(V-X)^4}{4} - \bar{k}_3 \frac{(V-X)^4}{4} + \bar{k}_4 \frac{(V-X)^8}{8} + k(L-L_o)^2 \quad (10)$$

where $X = \frac{B}{\omega}$ and $V = \frac{A}{\omega}$, the FEP is generated as shown in Fig. 3.

The periodic motions on the backbones and their associated low and high frequency subharmonic branches are represented by nonlinear normal modes (NNMs) in the configuration space. The frequency content in backbones and the subharmonic branches is characterized here by the frequency ratio between the LO and BNES periodic oscillations. The frequency indices $Snm\pm$ and $Unm\pm$ indicate symmetrical and unsymmetrical periodic motions, respectively, on the backbones and subharmonic branches. In $Snm\pm$ and $Unm\pm$, nm indicates to the resonance frequency ratio $(n:m)$ in the periodic motion between the LO and BNES masses where the plus sign $(+)$ indicates to in phase and the minus sign $(-)$ indicates to anti-phase motions.

As we will discuss in the next section, the FEP was also generated by numerical continuation using the method described in [47-48]. In Fig. 3, we compare the periodic solutions on the backbone branches S11+ and S13– of the LO-BNES system generated by the analytical approximation using CX-A technique to the exact FEP obtained by the numerical continuation method with $k = 0.14\mathrm{N/m}$ and $L_0 = 0.882L$. The log-scale in energy axis is avoided in this figure to provide more feasible comparison. The figure clearly indicates good agreement at frequencies close to the natural frequency of LO and consistent matching as the frequency

increases. Detailed discussions of the exact numerically computed branches resulting from is presented in the next section.

The branches obtained by CX–A are plotted in Fig. 4 for varying stiffness k and length ratio L_0/L. First, it is important to note that changing the stiffness and/or the length ratio of the transversely coupled linear springs, which produce the bistability conditions and nonlinearity, have a significant effect on the global dynamics of the LO–BNES system. It is also noted that these changes have an effect on the topology of the unstable branches. This can be concluded from the width of the energy interval corresponding to the unstable solutions which is realized by the derivative of the total energy with respect to the frequency index (i.e. slope of Fig. 4). As shown in [35], this unstable part of the branch has a significant effect on the TET in the system. In addition, Fig. 5 shows the difference in FEP if we include up to cubic terms only in (4) as opposed to including up to seventh order stiffness terms as done in this study. The difference in the resulting FEP indicates the strong nonlinearities in the LO–BNES system and the importance of considering the additional nonlinear terms. To further study the exact global dynamical behavior of the system, the next section discuss the resulting branches from the exact numerical continuation approach.

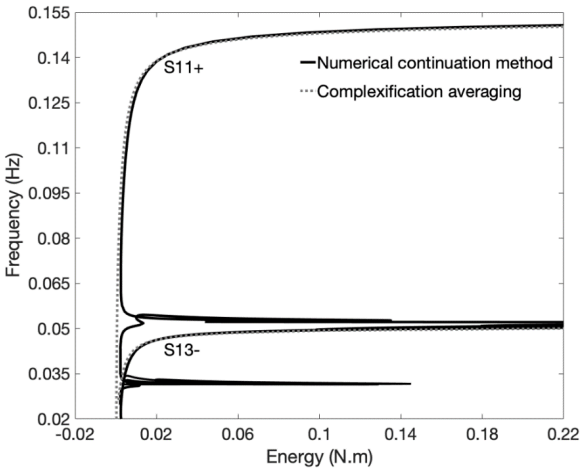

Fig. 3 FEP comparison of some branches generated by analytical (CX–A) and numerical continuation in the FEP of a LO–BNES with $\varepsilon = 0.05, k = 0.14N/m$ and $L0 = 0.882L$

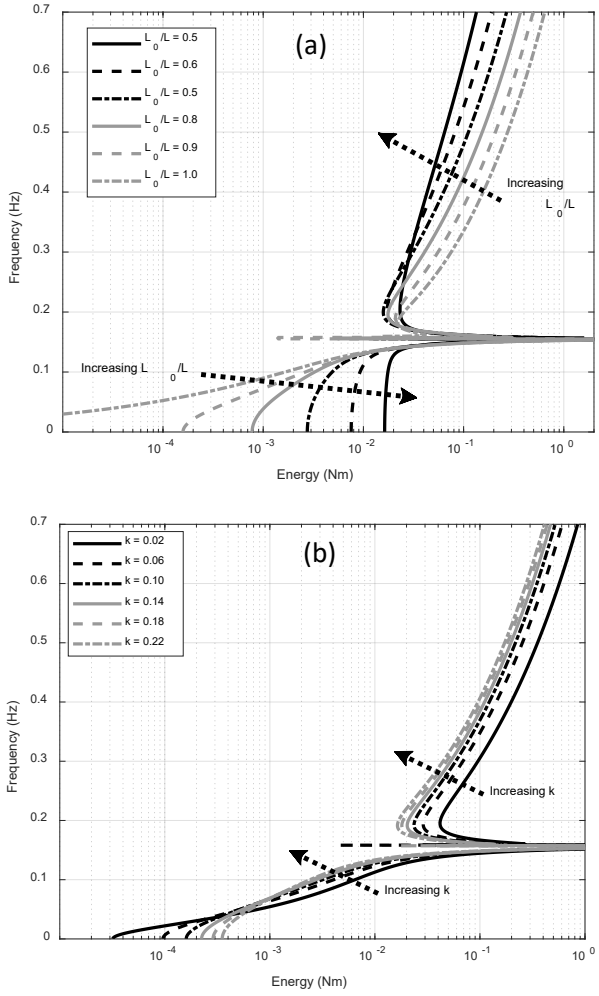

Fig. 4 Comparison of the backbone branch S11± in the approximate FEP generated by CX–A for a LO–BNES system with $\varepsilon = 0.05$ for (a) varying length ratio L_0/L with $k = 0.14N/m$ and (b) for varying stiffness k with $L_0 = 0.882$

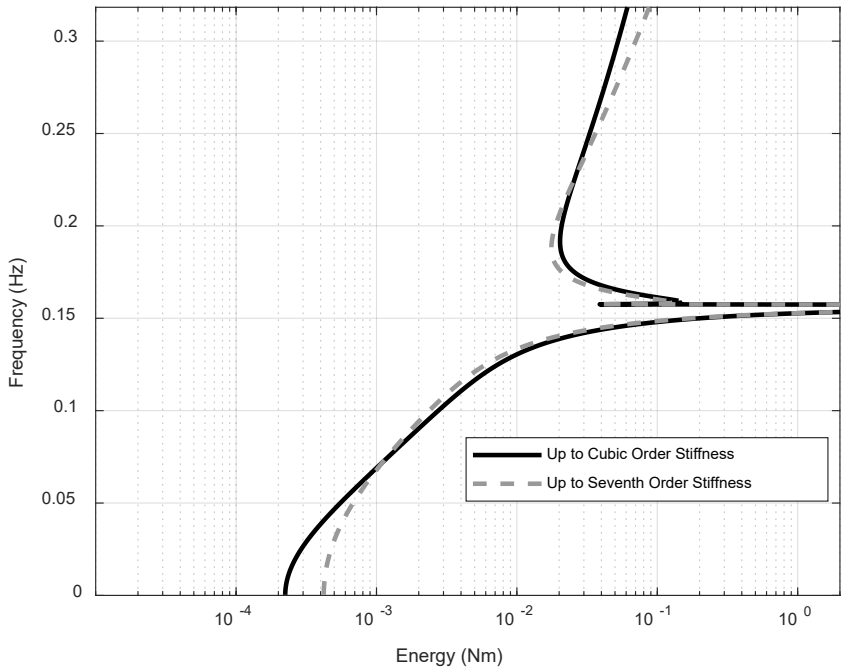

Fig. 5 Comparison of the backbone branch S11± in the approximate FEP generated by CX–A for a LO–BNES system with $\varepsilon = 0.05, k = 0.14N/m$ and $L0 = 0.882L$ when considering up to cubic and seventh stiffness terms in (4)

FEP via numerical continuation

The FEP backbones and their associated subharmonic resonance branches are constructed here based on the numerical continuation method described in [47-48]. All FEP backbones and their associated subharmonic branches are obtained for nonzero initial displacements and zero initial velocities in (3).

The fundamental FEP backbone of 1:1 in phase resonance ($S11+$) and its associated tongues of subharmonic resonances is shown in Fig. 6. Several symmetrical anti-phase subharmonic resonance branches are also obtained on this backbone as shown in the figure near to the LO natural frequency ($f_{LO} = 0.1592$ Hz) and to 1/3 of this frequency. These branches are expressed by $S13-$, $S15-$ and $S17-$. Examples of periodic motions on S11+ and their associated NNMs in the

configuration space are shown in Fig. 7 where full NES oscillation through the equilibrium positions takes place.

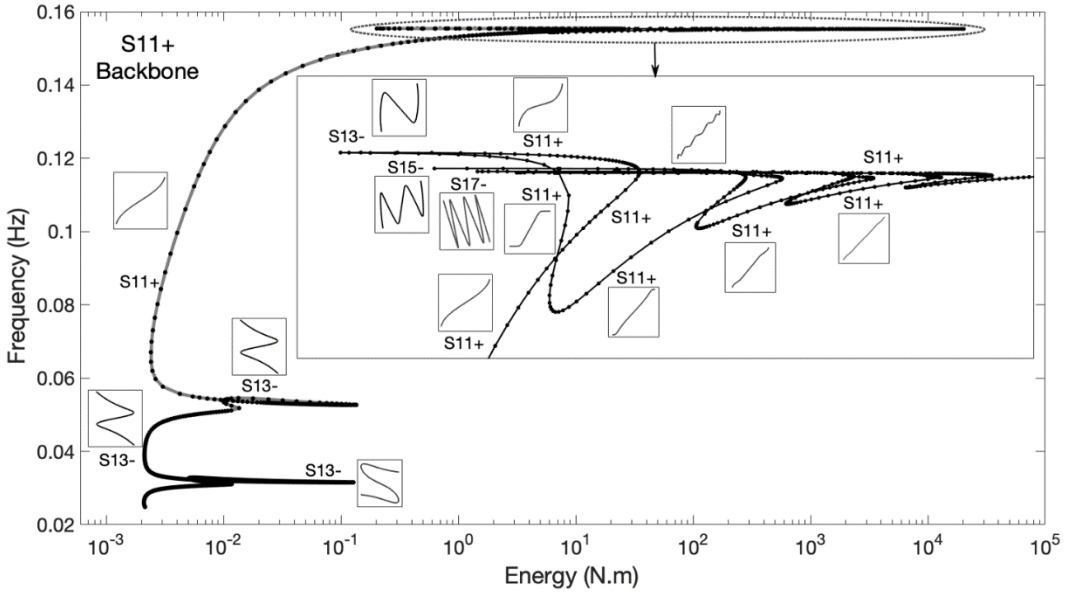

Fig. 6 The frequency energy plot of the fundamental $S11+$ backbone and its associated subharmonic branches for the LO-BNES system.

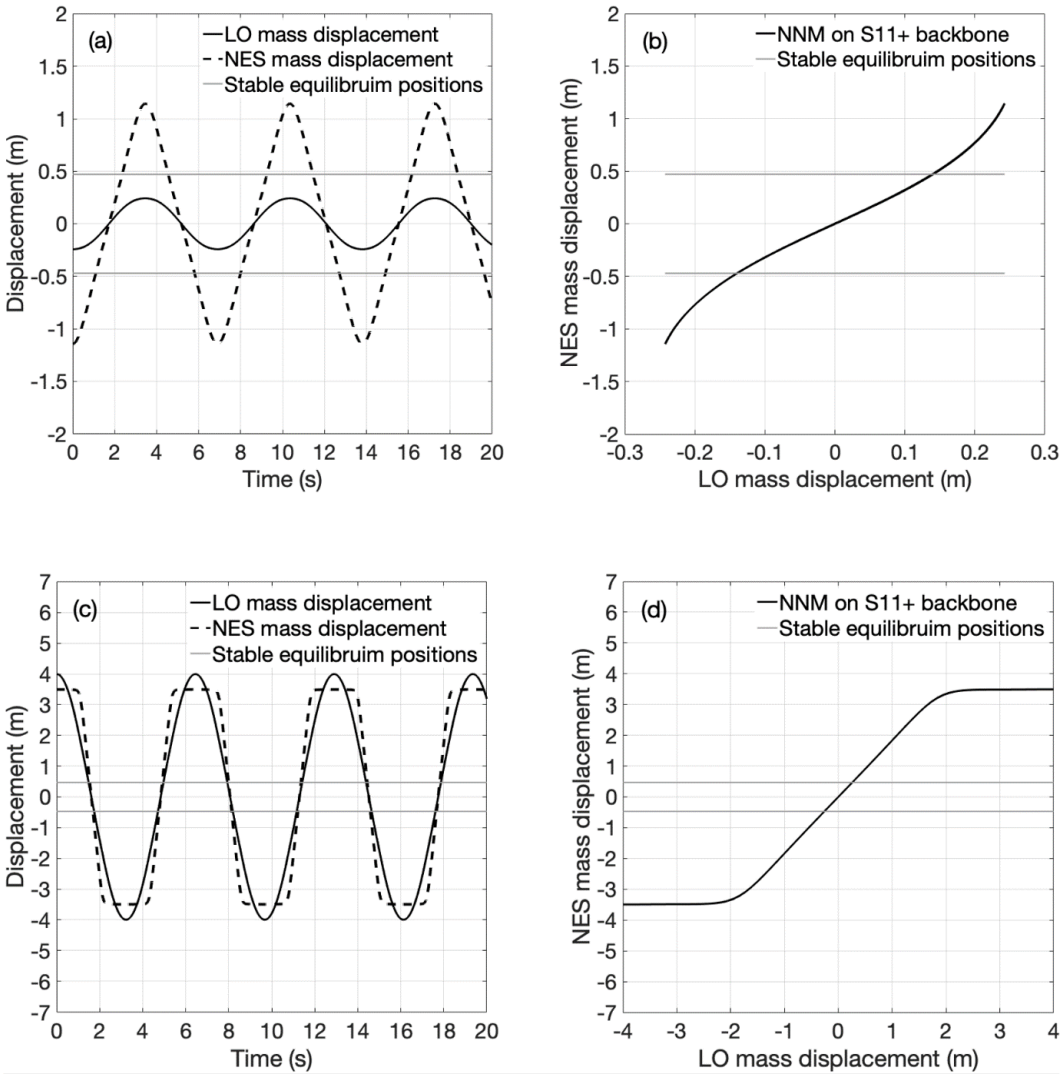

Fig. 7 The periodic motions in (a) and (c) and their corresponding NNMs in (b) and (d) for two different initial conditions on the $S11+$ backbone of the FEP.

Another $S11+$ backbone curve of similar behavior of the fundamental $S11+$ backbone has been obtained and plotted in Fig. 8. Symmetrical anti-phase subharmonic resonance branches are also obtained on this backbone as shown in the figure near to the 1/3 of the LO natural frequency where these branches are represented by $S13-$ and $S15-$. Examples of periodic motions on these subharmonic branches and their associated NNMs are shown in Fig. 9 where full BNES oscillation through the equilibrium positions takes place.

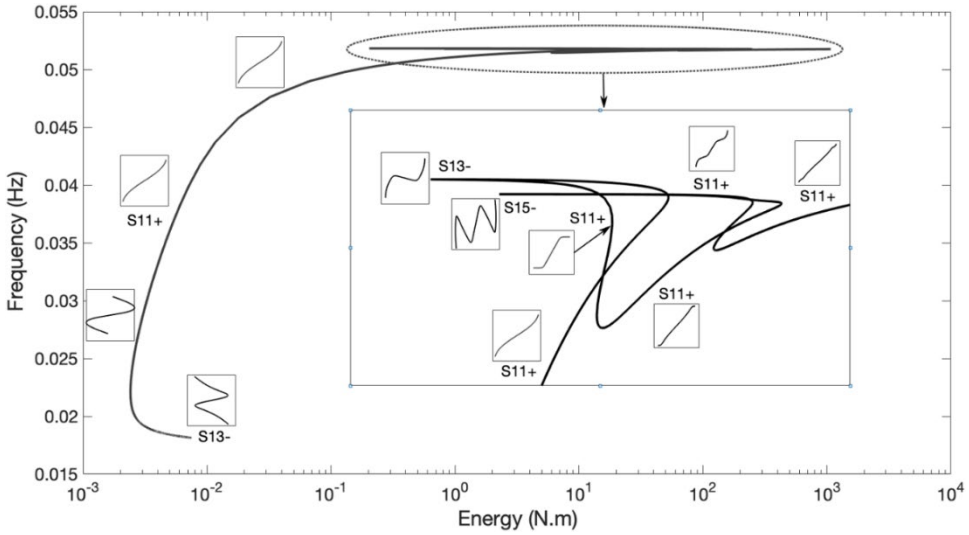

Fig. 8 The frequency energy plot of the second $S11+$ backbone and its associated subharmonic branches for the LO-BNES system.

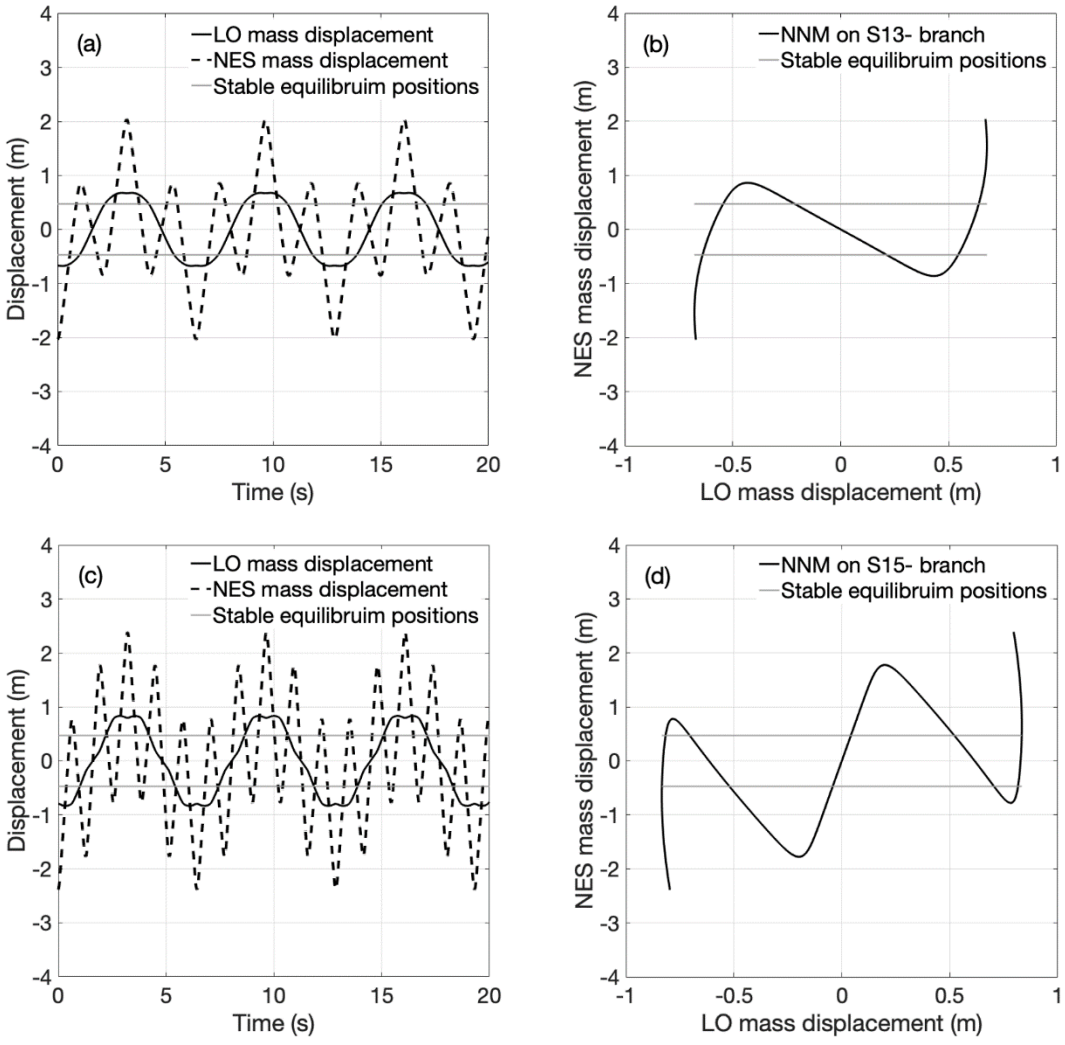

Fig. 9 The periodic motions and their corresponding NNMs on the second $S11+$ backbone subharmonic branches $S13-$ in (a) and (b) and $S15-$ in (c) and (d).

Unlike the NES with purely nonnegative cubic coupling stiffness, the BNES is associated with several unsymmetrical backbones ($U11+$ and $U11-$) of 1:1 resonance which appear to the left zone of $S11+$ and $S11-$ backbones at low energy as shown in the FEP in Fig. 10. This interesting finding shows the rich nonlinear dynamical behavior of the bistable attachment and its high efficiency in energy harvesting and vibration suppression compared with other types of NESs. Moreover, three $S11-$ backbones are also obtained and shown in the same plot. Unlike the $S11+$ and $S11-$ backbones, the frequency on the $U11+$ and the $U11-$ backbones decreases with increasing the energy. It is also observed that at these unsymmetrical backbones, the periodic oscillation at 1:1 resonance occurs only about one of the BNES equilibrium positions ($z = \pm z_c$). This means that, passing through the unstable equilibrium position (at $z = 0$) during the periodic oscillation does not exist at these unique BNES backbones. This important finding shows that both NES and LO periodic motions can occur at wide range of nonlinear frequency at low energy content.

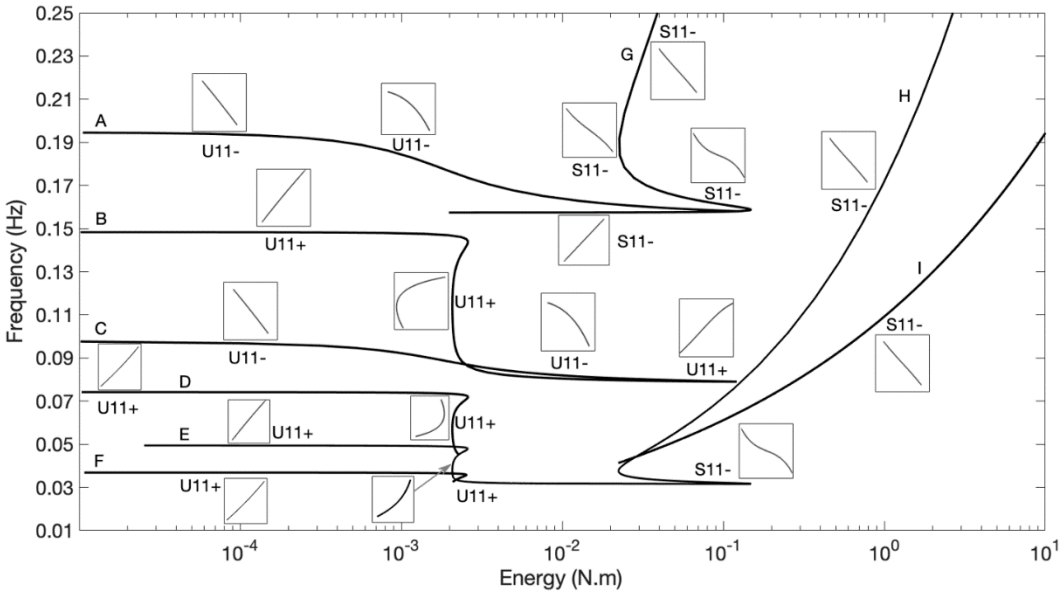

Fig. 10 The frequency energy plots of $U11+$, $U11-$ and $S11-$ backbones.

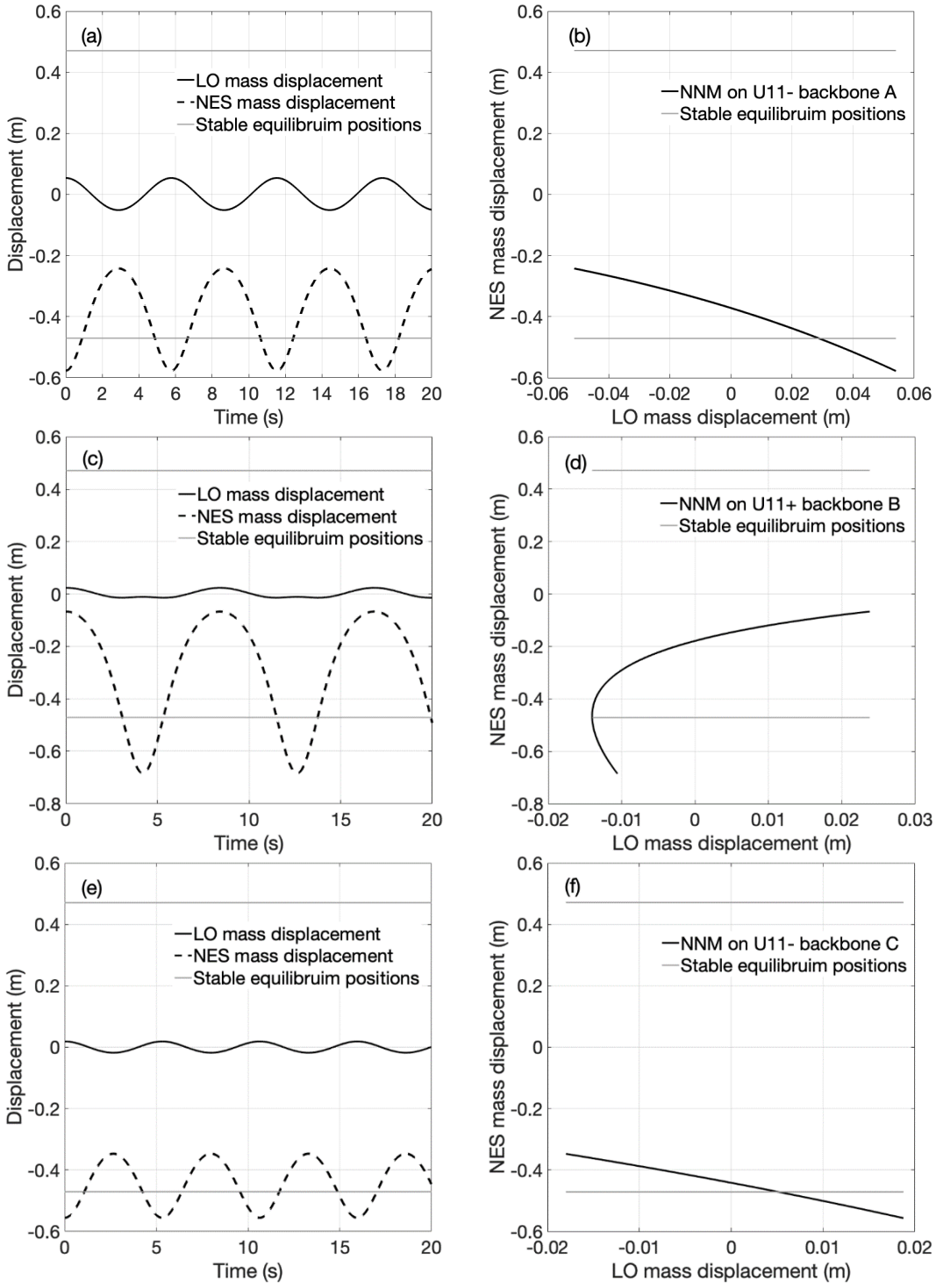

Fig. 11 Periodic motions and their corresponding NNMs, respectively, in (a) and (b) at $U11-$ backbone A, in (c) and (d) at $U11+$ backbone B and in (e) and (f) at $U11-$ backbone C.

Examples of the periodic motion of LO-BNES system on $U11+$ and $U11-$ backbones named A, B and C in Fig. 10 are shown in Fig. 11. Both masses depict an out of phase periodic oscillation at the $U11-$ backbone A as shown from the

response and the NNM in Fig. 10a and 10b, respectively. Similar observations are depicted from Figs. 10b and 10c at $U11+$ backbone B and from Figs. 10e and 10f at $U11-$ backbone C. In these figures the BNES mass oscillates about its left equilibrium position where the passage through the unstable equilibrium position does not occur.

Finally, the damped dynamics of the LO-BNES system is investigated by imposing the wavelet transform frequency spectrum on the full FEP. The wavelet frequency content of the relative NES displacement response is imposed into the FEP for different initial conditions and damping parameters as shown in Figs. 12 and 13. In Fig. 12 the BNES mass exhibits a strong resonance capture with the LO mass on the $U11-$ backbone A and $U11+$ backbone B as shown in Fig. 12 a. However, this resonance capture occurs at three different parts of backbones A and B in Fig. 12b when the initial energy slightly elevated. The imposed wavelet spectrums on $S11+$ and $S11-$ fundamental backbones are shown in Fig. 13. The strong resonance capture between the NES mass and LO oscillations at these backbones indicate the accuracy of the numerical simulation for generating the FEP.

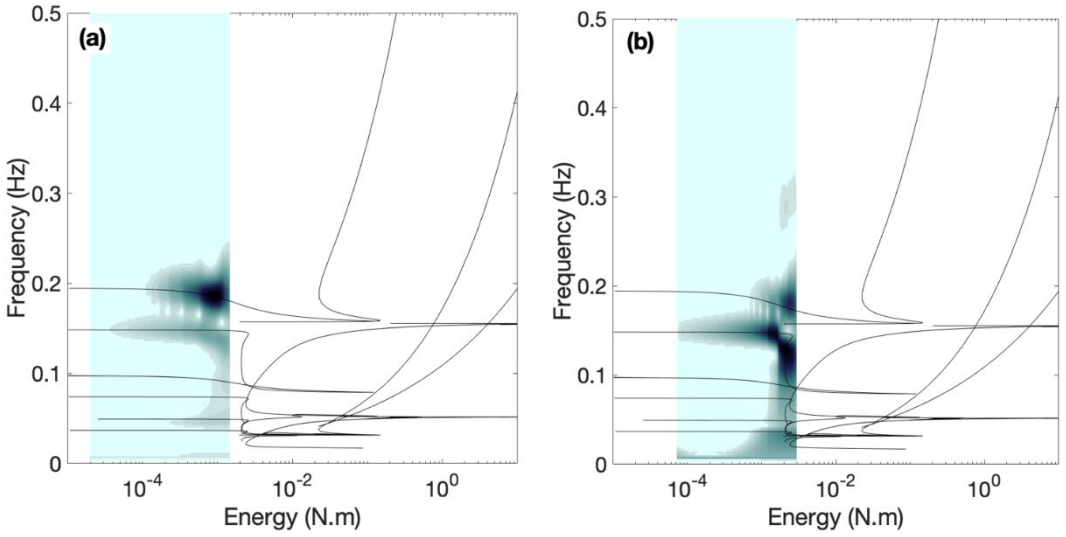

Fig. 12 Imposed wavelet transforms of the relative displacement of the NES mass in the LO-BNES system at $\dot{x}_1(0) = 0.22$ m/s , $\dot{x}_2(0) = -0.022$ m/s in (a) and at $\dot{x}_1(0) = 0.075$ m/s , $\dot{x}_2(0) = -0.075$ m/s in (b) for $\lambda = 0.002$ N·s/m and $\lambda_p = 0.001$ N·s/m .

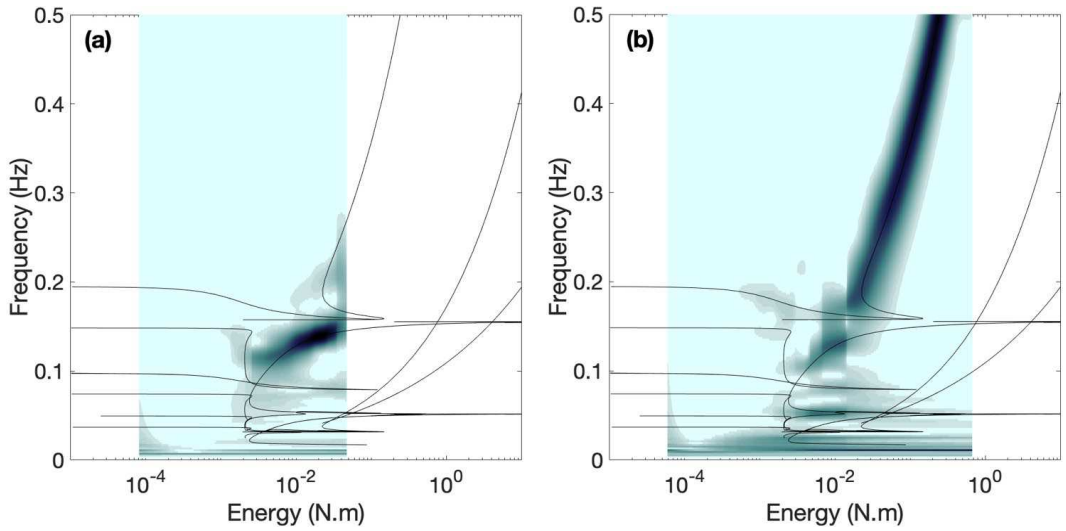

Fig. 13 Imposed wavelet transforms of the relative displacement of the NES mass in the LO-BNES system at $\dot{x}_1(0) = -0.3$ m/s , $\dot{x}_2(0) = -0.3$ m/s in (a) and at $\dot{x}_1(0) = 5$ m/s , $\dot{x}_2(0) = -0.3$ m/s for $\lambda = 0.002$ N·s/m , $\lambda_p = 0.001$ N·s/m .

Concluded Remarks

The Hamiltonian and damped dynamics of the bistable NES (BNES) attachment with a linear oscillator are investigated using FEPs obtained by analytical and numerical methods where the fundamental in-phase and out-of-phase

backbones have been obtained. The complexification-averaging (CX–A) technique is applied to the Hamiltonian system and the characteristics of the transverse springs on the resulting FEPs is found to affect the stability and topology of the branches which indicates the importance of the exact physical realization of the system. Following that, numerical continuation techniques are utilized to generate exact FEPs of the Hamiltonian LO–BNES system which included multiple symmetrical and unsymmetrical in- and out of-phase backbone branches. It is found that new 1:1 in phase and out of phase periodic oscillations occur on unsymmetrical NNMs backbone branches. On these unsymmetrical NNMs backbones, the BNES has been found to periodically oscillate at 1:1 resonance with the linear structure about its one of stable equilibrium position. Moreover, passage of BNES mass through its unstable equilibrium position does not occur at these unsymmetrical NNMs backbones. Imposing the wavelet shows the strong resonance capture between the NES mass and LO oscillations indicating the accuracy of the numerical simulation for generating the FEP.

Conflict of Interest

The authors declare that they have no conflict of interest.

References

[1] Vakakis, A. F., Gendelman, O. V., Bergman, L. A., McFarland, D. M., Kerschen, G., Lee, Y. S.: Nonlinear targeted energy transfer in mechanical and structural systems, Vol. 156. Springer Science & Business Media (2008).

[2] Gendelman, O., Manevitch, L., Vakakis, A.F., Mcloskey, R.: Energy pumping in nonlinear mechanical oscillators: Part I dynamics of the underlying hamiltonian systems. J. Appl. Mech. **68**(1), 34–41 (2001). https://doi.org/10.1115/1.1345524

[3] Vakakis, A.F., and Gendelman, O.: Energy pumping in nonlinear mechanical oscillators: part II resonance capture. J. Appl. Mech. **68**(1), 42–48 (2001). https://doi.org/10.1115/1.1345525

[4] Lee, Y.S., Kerschen, G., Vakakis, A.F., Panagopoulos, P., Bergman, L., McFarland, D.M.: Complicated dynamics of a linear oscillator with a light, essentially nonlinear attachment. Physica D: Nonlinear Phenomena **204**(1-2), 41–69 (2005). https://doi.org/10.1016/j.physd.2005.03.014

[5] Quinn, D.D., Gendelman, O., Kerschen, G., Sapsis, T.P., Bergman, L.A., Vakakis, A.F.: Efficiency of targeted energy transfers in coupled nonlinear oscillators associated with 1: 1 resonance captures: Part I. J. Sound Vib. **311**(3-5), 1228–1248 (2008). https://doi.org/10.1016/j.jsv.2007.10.026

[6] Sapsis, T., Vakakis, A.F., Gendelman, O.V., Bergman, L.A., Kerschen, G., Quinn, D.: Efficiency of targeted energy transfers in coupled nonlinear oscillators associated with 1: 1 resonance captures: Part II, analytical study. J. Sound Vib. **325**(1-2), 297– 320 (2009). https://doi.org/10.1016/j.jsv.2009.03.004

[7] Gourdon, E., Alexander, N. A., Taylor, C.A., Lamarque, C.-H., Pernot, S.: Nonlinear energy pumping under transient forcing with strongly nonlinear coupling: Theoretical and experimental results. J. Sound Vib. **300**(3-5), 522–551 (2007). https://doi.org/10.1016/j.jsv.2006.06.074

[8] McFarland, D.M., Bergman, L.A., Vakakis, A.F.: Experimental study of non-linear energy pumping occurring at a single fast frequency. Int. J. Non-Linear Mech. **40**(6), 891–899 (2005). https://doi.org/10.1016/j.ijnonlinmec.2004.11.001

[9] Sapsis, T.P., Quinn, D.D., Vakakis, A.F., Bergman, L.A.: Effective stiffening and damping enhancement of structures with strongly nonlinear local attachment. J. Vib. Acoust. ASME **134**(1), 011016 (2012). https://doi.org/10.1115/1.4005005

[10] Benacchio, S., Malher, A., Boisson, J., Touzé, C.: Design of a magnetic vibration absorber with tunable stiffnesses, Nonlinear Dyn. **85**, 893–911 (2016). https://doi.org/10.1007/s11071-016-2731-3

[11] Kremer, D., Liu, K.: A nonlinear energy sink with an energy harvester: Transient responses, J. Sound Vib. **333**(20), 4859–4880 (2014). https://doi.org/10.1016/j.jsv.2014.05.010

[12] Lo Feudo, S., Touzé, C., Boisson, J., Cumunel, G.: Nonlinear magnetic vibration absorber for passive control of a multi–storey structure, J. Sound Vib. **438**, 33–53 (2019). https://doi.org/10.1016/j.jsv.2018.09.007

[13] Ahmadi, M., Attari, N.K., Shahrouzi, M.: Structural seismic response mitigation using optimized vibro-impact nonlinear energy sinks. Journal of Earthquake Engineering **19**(2), 193–219 (2015). https://doi.org/10.1080/13632469.2014.962671

[14] Gendelman, O.V.: Analytic treatment of a system with a vibro-impact nonlinear energy sink. J. Sound Vib. **331**(21), 4599–4608 (2012). https://doi.org/10.1016/j.jsv.2012.05.021

[15] Li, T., Lamarque, C.H., Seguy, S., Berlioz, A.: Chaotic characteristic of a linear oscillator coupled with vibro-impact nonlinear energy sink. Nonlinear Dyn. **91**, 2319–2330 (2018). https://doi.org/10.1007/s11071-017-4015-y

[16] Li, T., Seguy, S., Berlioz, A.: On the dynamics around targeted energy transfer for vibro-impact nonlinear energy sink. Nonlinear Dyn. **87**, 1453-1466 (2017). https://doi.org/10.1007/s11071-016-3127-0

[17] Li, T., Seguy, S., Berlioz, A.: Optimization mechanism of targeted energy transfer with vibro-impact energy sink under periodic and transient excitation. Nonlinear Dyn. **87**, 2415–2433 (2017). https://doi.org/10.1007/s11071-016-3200-8

[18] Pennisi, G., Stephan, C., Gourc, E., Michon, G., Experimental investigation and analytical description of a vibro-impact NES coupled to a single-degree-of-freedom linear oscillator harmonically forced. Nonlinear Dyn. **88**,1769–1784 (2017). https://doi.org/10.1007/s11071-017-3344-1

[19] Wierschem, N.E., Hubbard, S.A., Luo, J., Fahnestock, L.A., Spencer, B.F., McFarland, D.M., Quinn, D.D., Vakakis, A.F., Bergman, L.A.: Response attenuation in a large-scale structure subjected to blast excitation utilizing a system of essentially nonlinear vibration absorbers. J. Sound Vib. **389**, 52–72 (2017). https://doi.org/10.1016/j.jsv.2016.11.003

[20] Li, W., Wierschem, N.E., Li, X., Yang, T.: On the energy transfer mechanism of the single-sided vibro-impact nonlinear energy sink. J. Sound Vib. **437**, 166–179 (2018). https://doi.org/10.1016/j.jsv.2018.08.057

[21] Al-Shudeifat, M.A., Saeed, A.S.: Comparison of a modified vibro-impact nonlinear energy sink with other kinds of NESs, Mecannica (2020). https://doi.org/10.1007/s11012-020-01193-3

[22] Sigalov, G., Gendelman, O.V., AL-Shudeifat, M.A., Manevitch, L.I., Vakakis, A.F., Bergman, L.A.: Resonance captures and targeted energy transfers in an inertially-coupled rotational nonlinear energy sink, Nonlinear Dyn. **69**, 1693–1704 (2012). https://doi.org/10.1007/s11071-012-0379-1

[23] AL-Shudeifat, M.A., Wierschem, N.E., Bergman, L.A., Vakakis, A.F.: Numerical and experimental investigations of a rotating nonlinear energy sink. Meccanica **52**, 763–779 (2017). https://doi.org/10.1007/s11012-016-0422-2

[24] Sigalov, G., Gendelman, O.V., AL-Shudeifat, M.A., Manevitch, L.I., Vakakis, A.F., Bergman, L.A.: Alternation of regular and chaotic dynamics in a simple two-degree-of-freedom system with nonlinear inertial coupling. Chaos: An Interdisciplinary Journal of Nonlinear Science **22**(1), 013118 (2012). https://doi.org/10.1063/1.3683480

[25] Gendelman, O.V., Sigalov, G., Manevitch, L.I., Mane, M., Vakakis, A.F., Bergman, L.A.: Dynamics of an eccentric rotational nonlinear energy sink. J. Appl. Mech. **79**(1), 011012 (2011). https://doi.org/10.1115/1.4005402

[26] Vorotnikov, K., Starosvetsky, Y.: Nonlinear energy channeling in the two-dimensional, locally resonant, unit-cell model. I. High energy pulsations and routes to energy localization. Chaos: An Interdisciplinary Journal of Nonlinear Science **25**(7), 073106 (2015). https://doi.org/10.1063/1.4922964

[27] Jayaprakash, K.R., Starosvetsky, Y.: Three-dimensional energy channeling in the unit-cell model coupled to a spherical rotator I: bidirectional energy channeling. Nonlinear Dyn. **89**, 2013–2040 (2017). https://doi.org/10.1007/s11071-017-3568-0

[28] Saeed, A.S., Al-Shudeifat, M.A., Vakakis, A.F.: Rotary-oscillatory nonlinear sink of robust performance. Int. J. Non-Linear Mech. **117**, 103249 (2019). https://doi.org/10.1016/j.ijnonlinmec.2019.103249

[29] Saeed, A.S., AL-Shudeifat, M.A., Cantwell, W.J., Vakakis, A.F.: Rotary-impact nonlinear energy sink for shock mitigation: analytical and numerical investigations. Arch. Appl. Mech. 90, 495–521 (2020). https://doi.org/10.1007/s00419-019-01622-0

[30] Manevitch L.I., Sigalov, G., Romeo, F., Bergman, L. A., Vakakis, A. F.: Dynamics of a linear oscillator coupled to a bistable light attachment: Analytical study. J. Appl. Mech. **81**(4), 041011 (2014). https://doi.org/10.1115/1.4025150

[31] Romeo, F., Sigalov, G., Bergman, L. A., Vakakis, A. F.: Dynamics of a linear oscillator coupled to a bistable light attachment: Numerical study. J. Comput. Nonlinear Dyn. **10**(1), 011007 (2015). https://doi.org/10.1115/1.4027224

[32] AL-Shudeifat, M. A.: Highly efficient nonlinear energy sink. Nonlinear Dyn. **76**, 1905–1920 (2014). https://doi.org/10.1007/s11071-014-1256-x

[33] AL-Shudeifat, M.A., Saeed, A.S.: Frequency-energy dependence of the bistable nonlinear energy sink. In: ASME International Design Engineering Technical Conferences and Computers and Information in Engineering Conference, Volume 8: 29th Conference on Mechanical Vibration and Noise, p. V008T12A022. ASME, Cleveland, OH (2017). https://doi.org/10.1115/DETC2017-67780

[34] Qiu, D., Li, T., Seguy, S., Paredes, M.: Efficient targeted energy transfer of bistable nonlinear energy sink: application to optimal design. Nonlinear Dyn. **92**, 443–461 (2018). https://doi.org/10.1007/s11071-018-4067-7

[35] Dekemele, K., Van Torre, P., Loccufier, M.: Performance and tuning of a chaotic bi-stable NES to mitigate transient vibrations. Nonlinear Dyn. **98**, 1831–1851 (2019). https://doi.org/10.1007/s11071-019-05291-0

[36] Habib, G., Romeo, F.: The tuned bistable nonlinear energy sink. Nonlinear Dyn. **89**, 179–196 (2017). https://doi.org/10.1007/s11071-017-3444-y

[37] Fourotan, K., Jalali, A., Ahmadi, H.: Investigations of energy absorption using tuned bistable nonlinear energy sink with local and global potentials. J. Sound Vib. **447**, 155–169 (2019). https://doi.org/10.1016/j.jsv.2019.01.030

[38] Fang, X., Wen, J.H., Yin, J.F., Yu, D.L.: Highly efficient continuous bistable nonlinear energy sink composed of a cantilever beam with partial constrained layer damping. Nonlinear Dyn. **87**, 2677–2695 (2017). https://doi.org/10.1007/s11071-016-3220-4

[39] Yao, H., Wang, Y., Xie, L., Wen, B.: Bi-stable buckled beam nonlinear energy sink applied to rotor system. Mech. Syst. Signal Process. **138**, 106546 (2020). https://doi.org/10.1016/j.ymssp.2019.106546

[40] Yao, H., Wang, Y., Cao, Y., Wen, B.: Multi-stable nonlinear energy sink for rotor system. Int. J. Non-Linear Mech. **118**, 103273 (2020). https://doi.org/10.1016/j.ijnonlinmec.2019.103273

[41] Yang, T.Z., Liu, T., Tang, Y., Hou, S., Lv, X.F.: Enhanced targeted energy transfer for adaptive vibration suppression of pipes conveying fluid. Nonlinear Dyn. **97**, 1937–1944 (2019). https://doi.org/10.1007/s11071-018-4581-7

[42] Zhao, J., Ming, L., Wang, H., Kacem, N., Huang, Y., Liu, P.: Piezoelectric actuated nonlinear energy sink with tunable attenuation efficiency. J. Appl. Mech. **87**(2), 021003 (2020). https://doi.org/10.1115/1.4045108

[43] Tsakirtzis, S., Panagopoulos, P. N., Kerschen, G., Gendelman, O., Vakakis, A. F., Bergman, L. A.: Complex dynamics and targeted energy transfer in linear oscillators coupled to multi-degree-of-freedom essentially nonlinear attachments. Nonlinear Dyn. **48**(3), 285–318 (2007). https://doi.org/10.1007/s11071-006-9089-x

[44] Kerschen, G., Vakakis, A. F., Lee, Y. S., McFarland, D. M., Kowtko, J. J., Bergman, L. A.: Energy transfers in a system of two coupled oscillators with essential nonlinearity: 1: 1 resonance manifold and transient bridging orbits. Nonlinear Dyn. **42**(3), 283–303 (2005). https://doi.org/10.1007/s11071-005-4475-3

[45] Kerschen, G., Kowtko, J. J., McFarland, D. M., Bergman, L. A., & Vakakis, A. F.: Theoretical and experimental study of multimodal targeted energy transfer in a system of coupled oscillators. Nonlinear Dyn. **47**(1–3), 285–309 (2007). https://doi.org/10.1007/s11071-006-9073-5

[46] Kerschen, G., Peeters, M., Golinval, J.C.: Nonlinear normal modes, Part I: A useful framework for the structural dynamicist. Mech. Syst. Signal Process. **23**(1), 170–194 (2009). https://doi.org/10.1016/j.ymssp.2008.04.002

[47] Renson, L., Kerschen, G., Cochelin, B.: Numerical computation of nonlinear normal modes in mechanical engineering. J. Sound Vib. **364**, 177–206 (2016). https://doi.org/10.1016/j.jsv.2015.09.033

[48] Haris, A., Alevras, P., Mohammadpour, M., Theodossiades, S., O'Mahony, M.: Design and validation of a nonlinear vibration absorber to attenuate torsional oscillations of propulsion systems. Nonlinear Dyn. **100**, 33–49 (2020). https://doi.org/10.1007/s11071-020-05502-z

[49] Lee, Y. S., Nucera, F., Vakakis, A. F., McFarland, D. M., Bergman, L. A.: Periodic orbits, damped transitions and targeted energy transfers in oscillators with vibro-impact attachments. Physica D: Nonlinear Phenomena, **238**(18), 1868–1896 (2009). https://doi.org/10.1016/j.physd.2009.06.013

[50] Nucera, F., Vakakis, A. F., McFarland, D. M., Bergman, L. A., Kerschen, G.: Targeted energy transfers in vibro-impact oscillators for seismic mitigation. Nonlinear Dyn. **50**(3), 651–677 (2007). https://doi.org/10.1007/s11071-006-9189-7

[51] Li, T., Seguy, S., Berlioz, A.: Optimization mechanism of targeted energy transfer with vibro-impact energy sink under periodic and transient excitation. Nonlinear Dyn. **87**(4), 2415–2433 (2017). https://doi.org/10.1007/s11071-016-3200-8

[52] Tao, H., Gibert, J.: Periodic orbits of a conservative 2-DOF vibro-impact system by piecewise continuation: bifurcations and fractals. Nonlinear Dyn. **95**(4), 2963–2993 (2019). https://doi.org/10.1007/s11071-018-04734-4

[53] Singh, A., & Moore, K. J.. Characteristic nonlinear system identification of local attachments with clearance nonlinearities. Nonlinear Dyn. **102**(3), 1667–1684 (2020). https://doi.org/10.1007/s11071-020-06004-8

[54] Al-Shudeifat, M. A.: Analytical formulas for the energy, velocity and displacement decays of purely nonlinear damped oscillators. Journal of vibration and control **21**(6), 1210–1219 (2015). https://doi.org/10.1177/1077546313493817

[55] Al-Shudeifat, M. A.: Amplitudes decay in different kinds of nonlinear oscillators. Journal of vibration and acoustics **137**(3), 031012 (2015). https://doi.org/10.1115/1.4029288

[56] AL-Shudeifat, M. A.: Time-varying stiffness method for extracting the frequency–energy dependence in the nonlinear dynamical systems. Nonlinear Dyn. **89**(2), 1463–1474 (2017). https://doi.org/10.1007/s11071-017-3528-8

[57] Al-Shudeifat, M. A.: Modal damping variations in nonlinear dynamical systems. Nonlinear Dyn. **93**(4), 2565–2578 (2018). https://doi.org/10.1007/s11071-018-4342-7

[58] Manevitch L.I.:Complex Representation of Dynamics of Coupled Nonlinear Oscillators. In: Uvarova L.A., Arinstein A.E., Latyshev A.V. (eds) Mathematical Models of Non-Linear Excitations, Transfer, Dynamics, and Control in Condensed Systems and Other Media. Springer, Boston, MA (1999). https://doi.org/10.1007/978-1-4615-4799-0_24

Figures

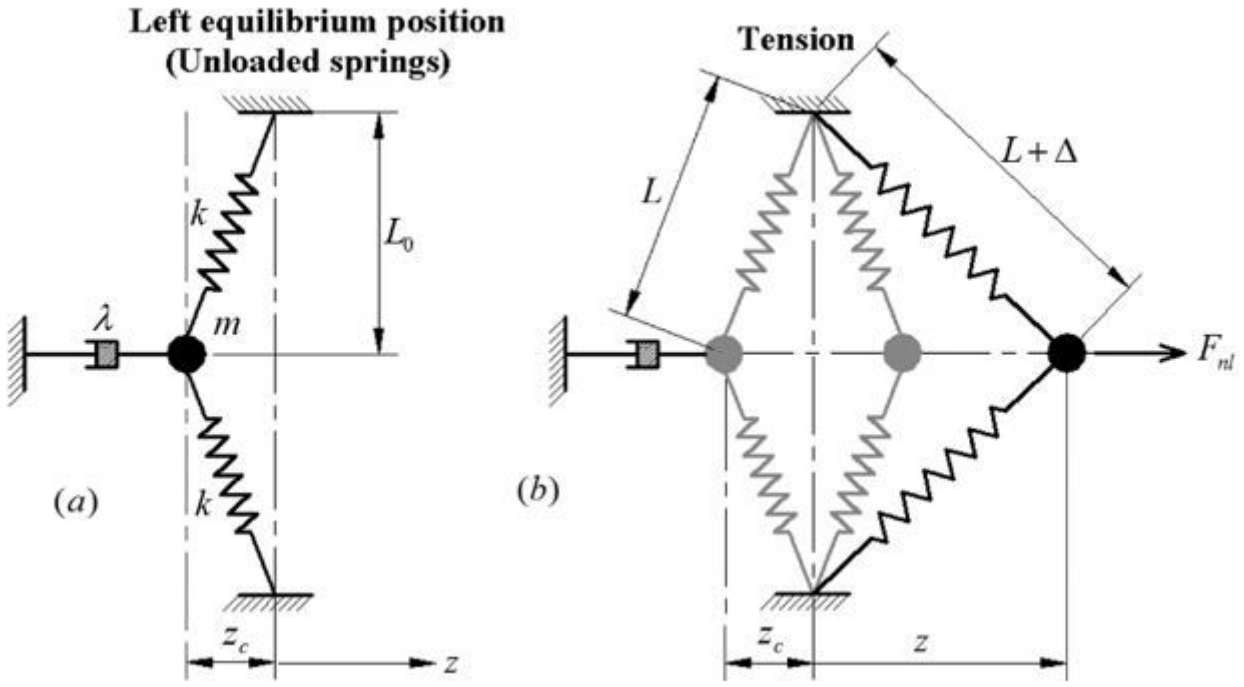

Figure 1

Physical configuration of the nonlinear damped oscillator.

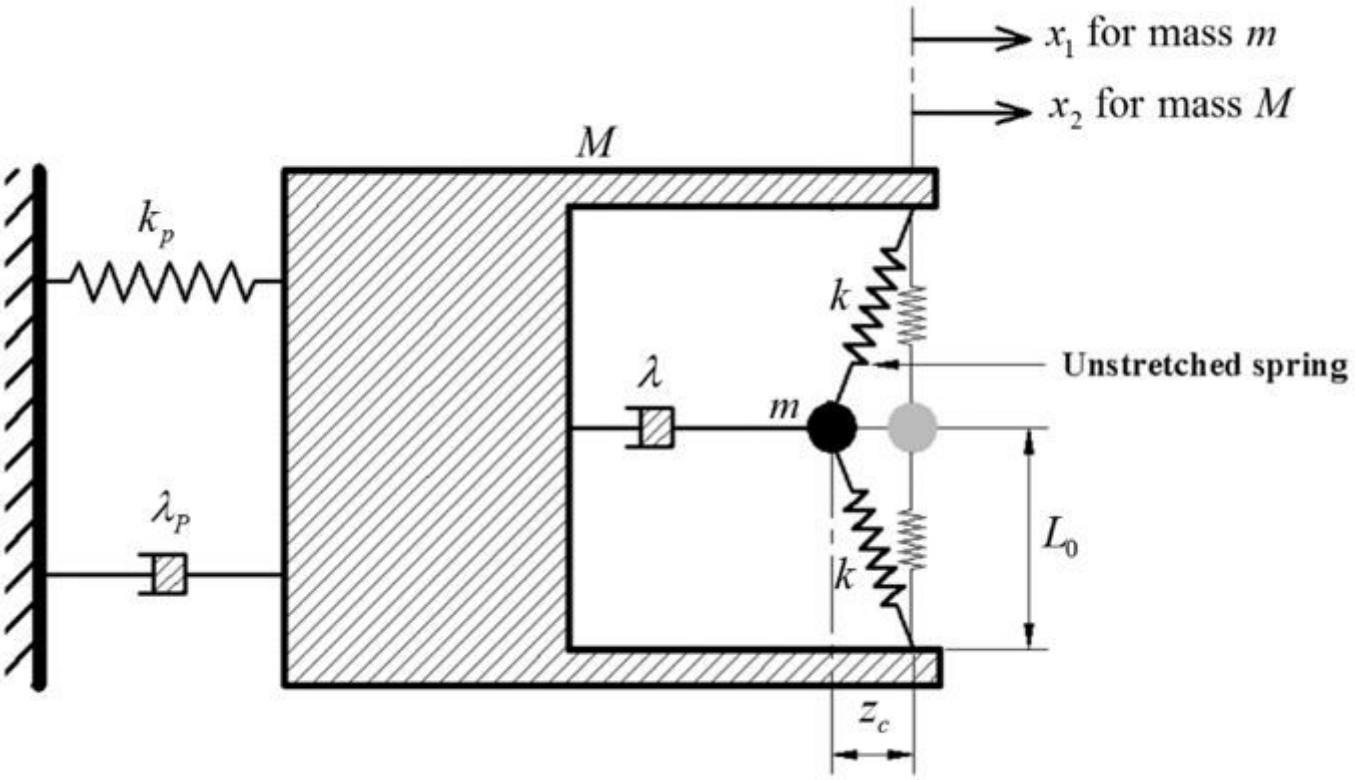

Figure 2

Single-degree-of freedom linear structure coupled to the modified NES.

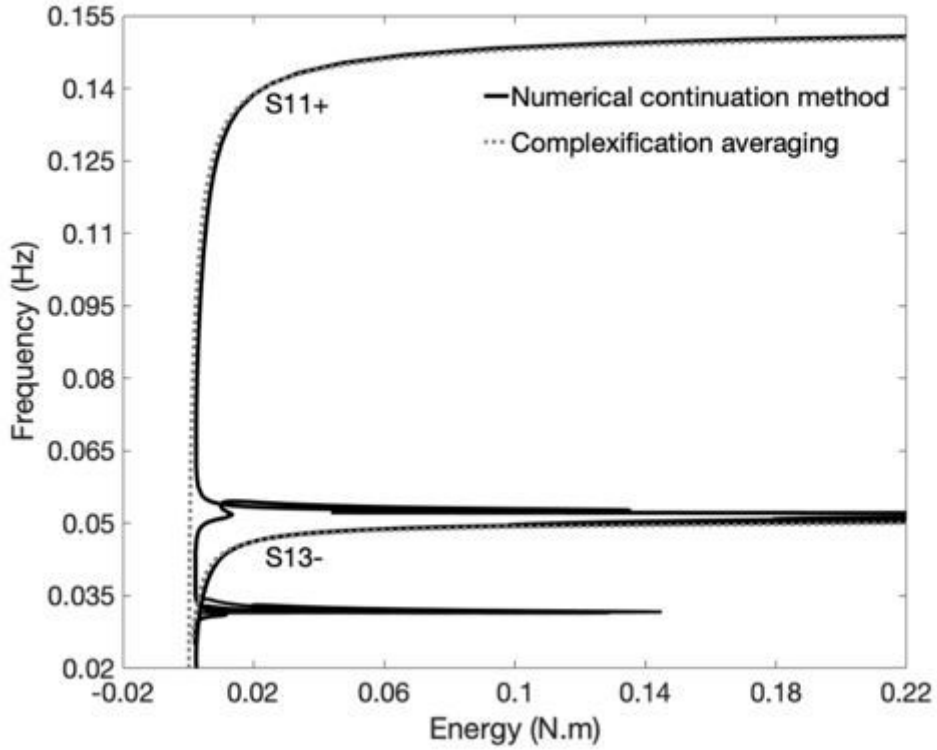

Figure 3

FEP comparison of some branches generated by analytical (CX−A) and numerical continuation in the FEP of a LO−BNES with ε=0.05,k=0.14N/m and L0=0.882L

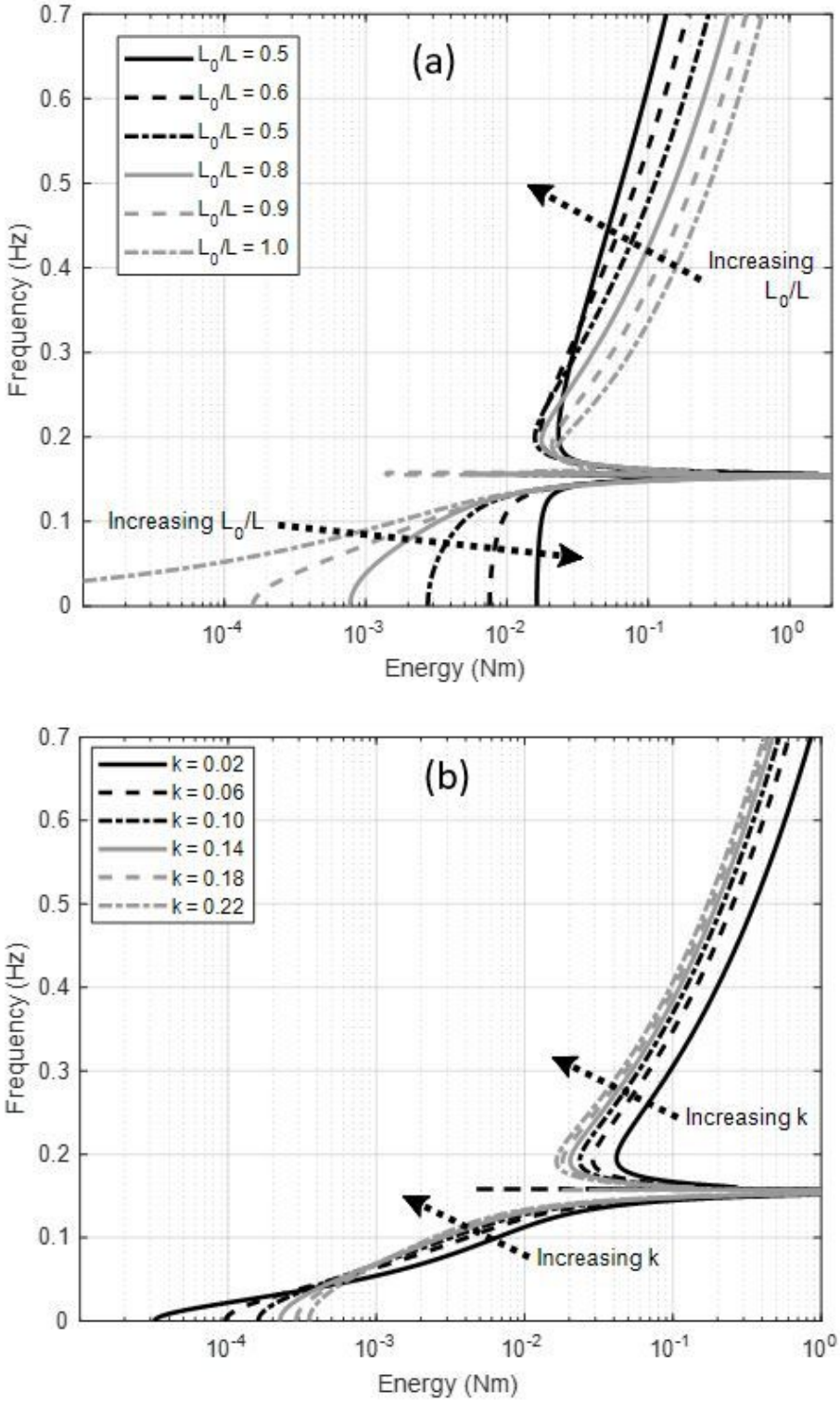

Figure 4

Comparison of the backbone branch S11± in the approximate FEP generated by CX–A for a LO–BNES system with ε=0.05 for (a) varying length ratio L_0/L with k=0.14N/m and (b) for varying stiffness k with L_0=0.882

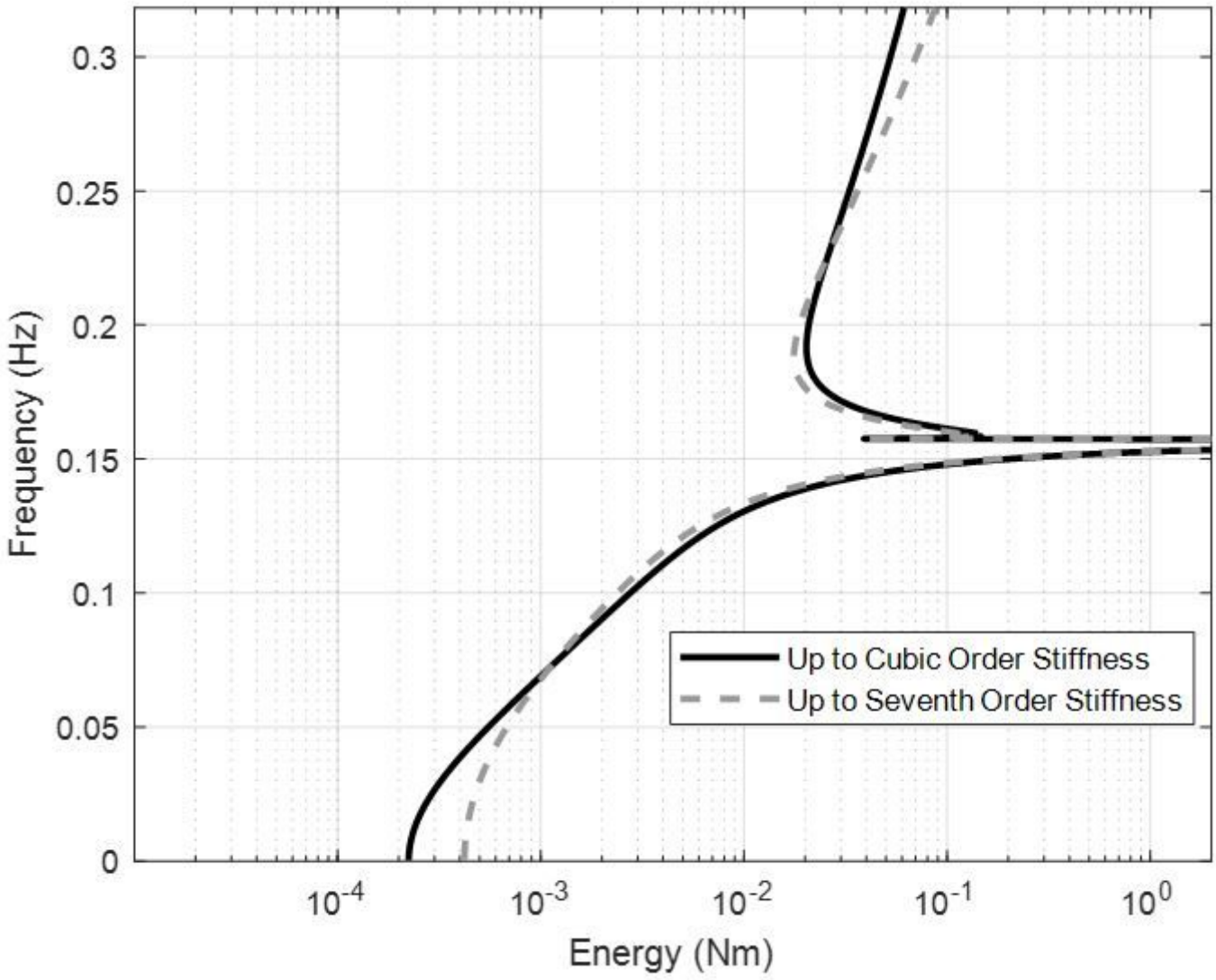

Figure 5

Comparison of the backbone branch S11± in the approximate FEP generated by CX–A for a LO–BNES system with ε=0.05,k=0.14N/m and L0=0.882L when considering up to cubic and seventh stiffness terms in (4)

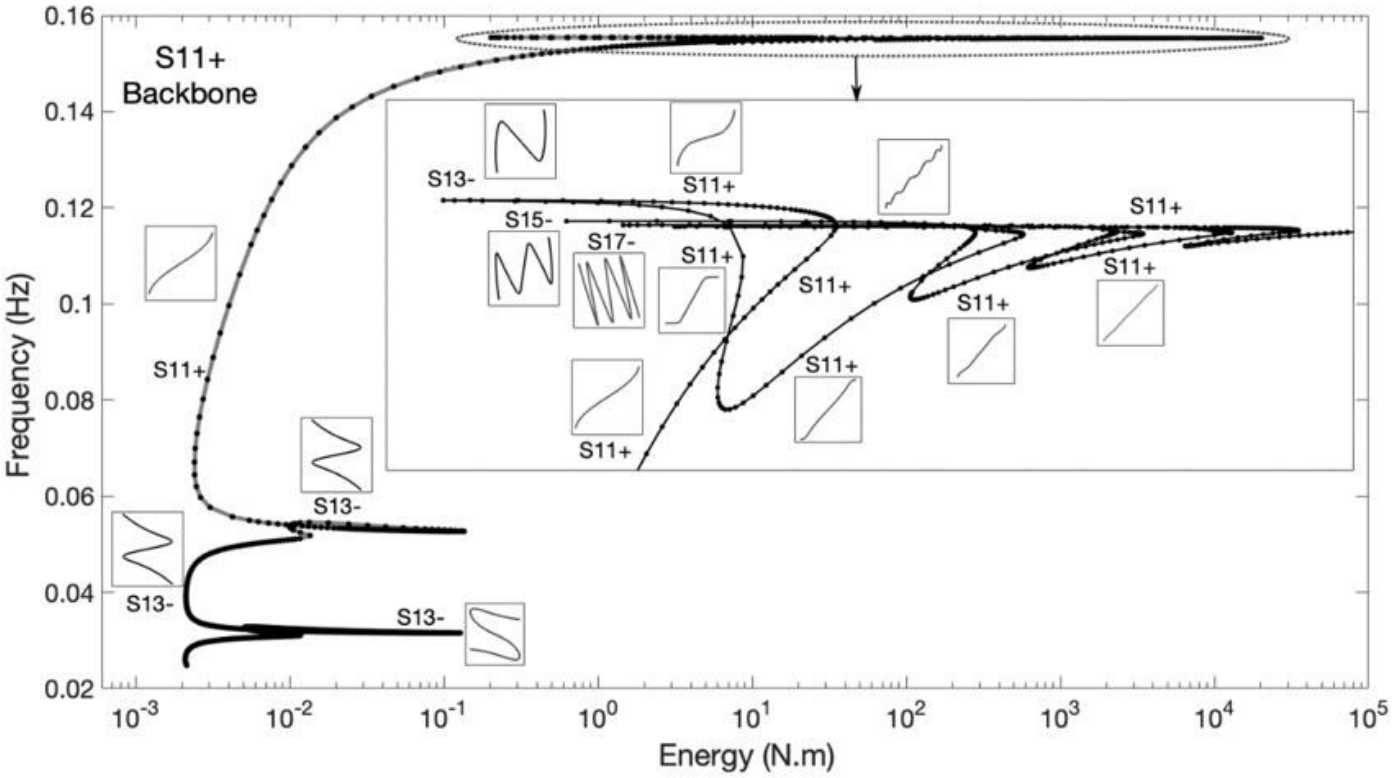

Figure 6

The frequency energy plot of the fundamental backbone and its associated subharmonic branches for the LO-BNES system.

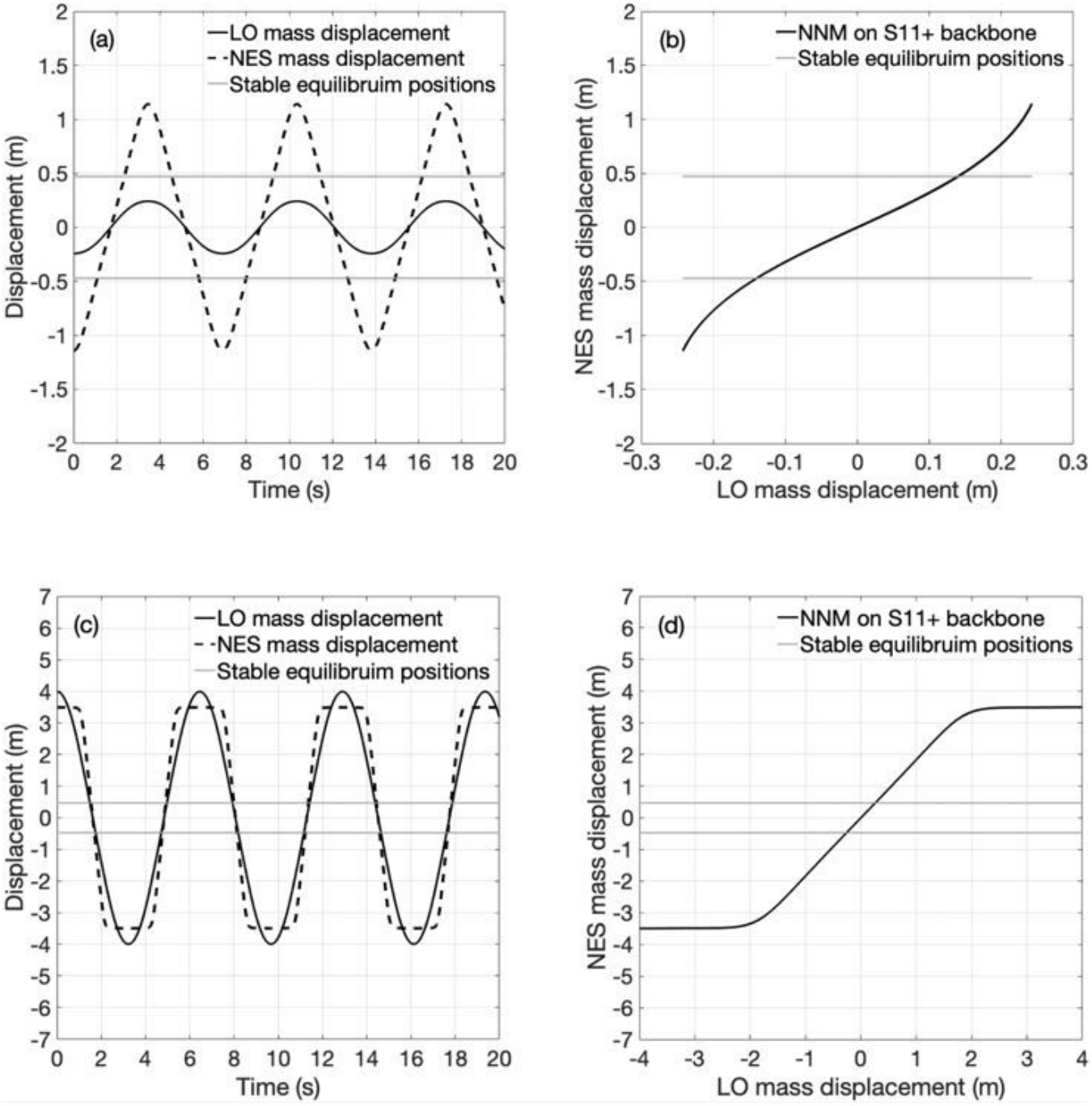

Figure 7

The periodic motions in (a) and (c) and their corresponding NNMs in (b) and (d) for two different initial conditions on the backbone of the FEP.

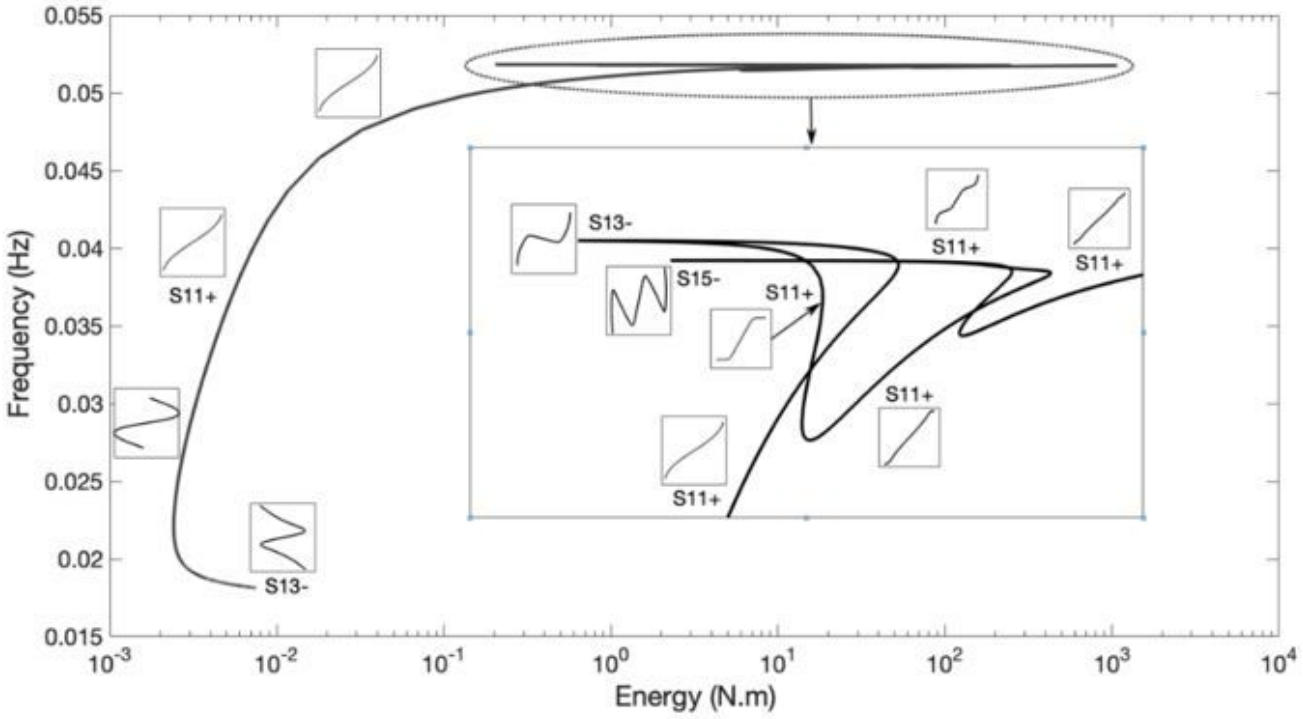

Figure 8

The frequency energy plot of the second backbone and its associated subharmonic branches for the LO-BNES system.

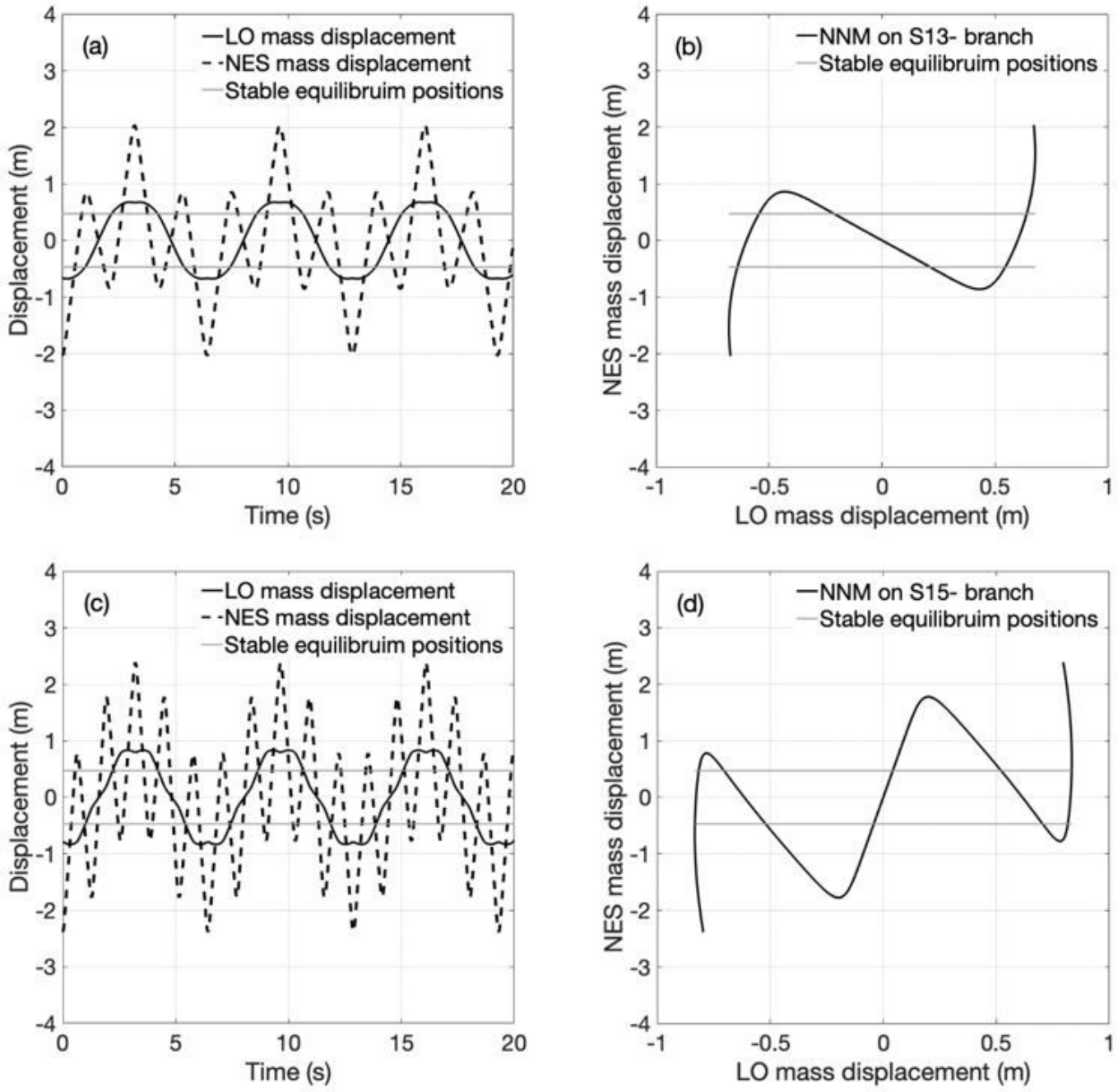

Figure 9

Caption for figure 9 can be found in the manuscript file.

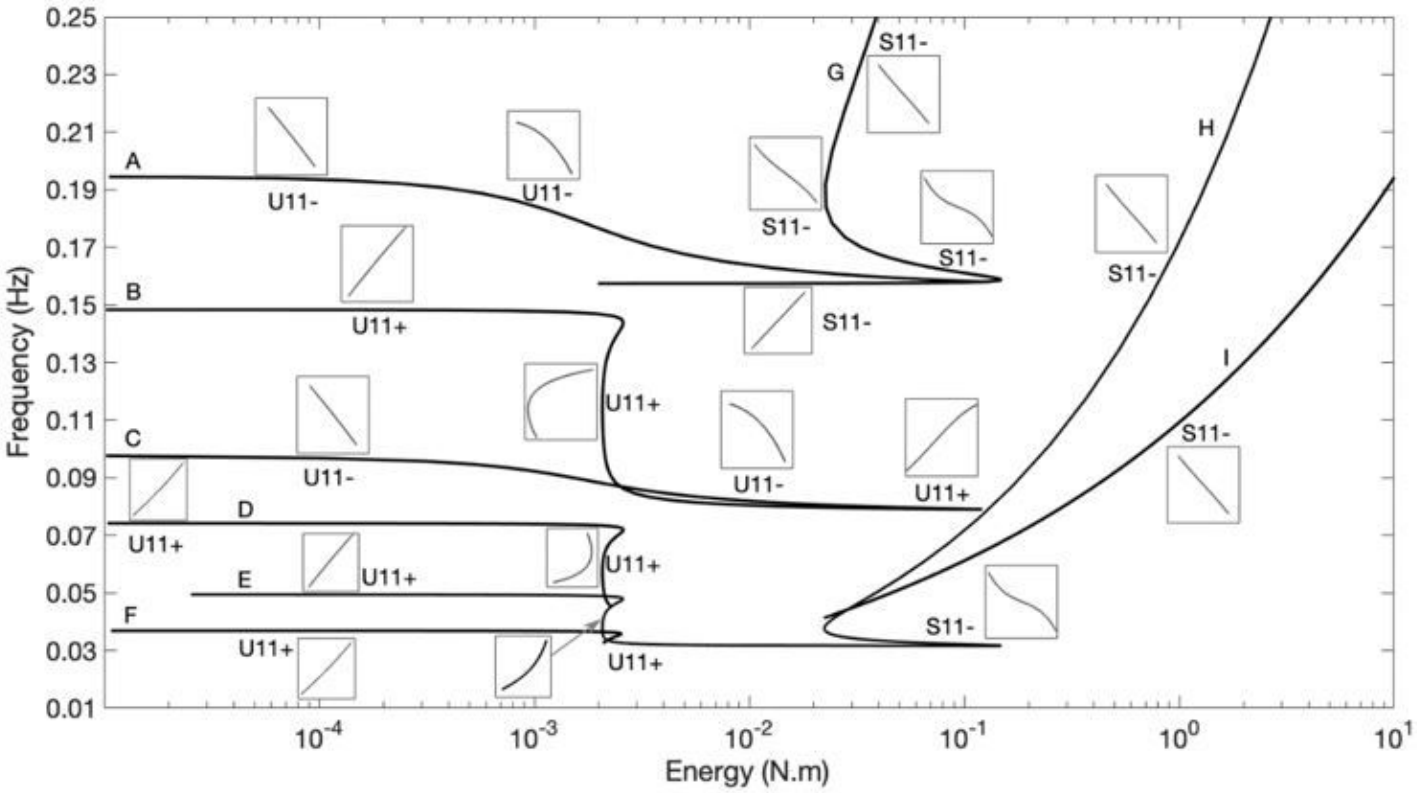

Figure 10

Caption for figure 10 can be found in the manuscript file.

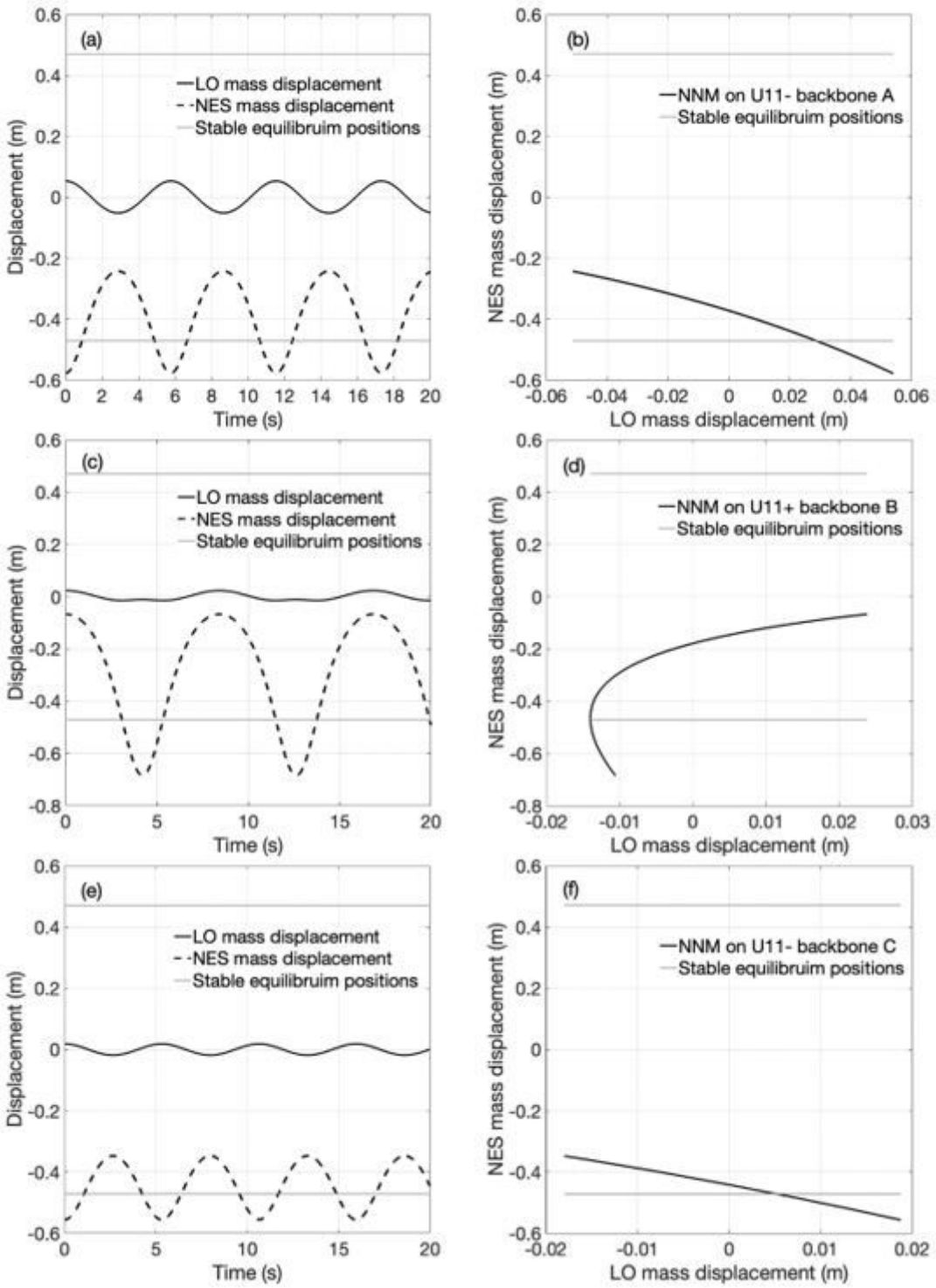

Figure 11

Periodic motions and their corresponding NNMs, respectively, in (a) and (b) at backbone A, in (c) and (d) at backbone B and in (e) and (f) at backbone C.

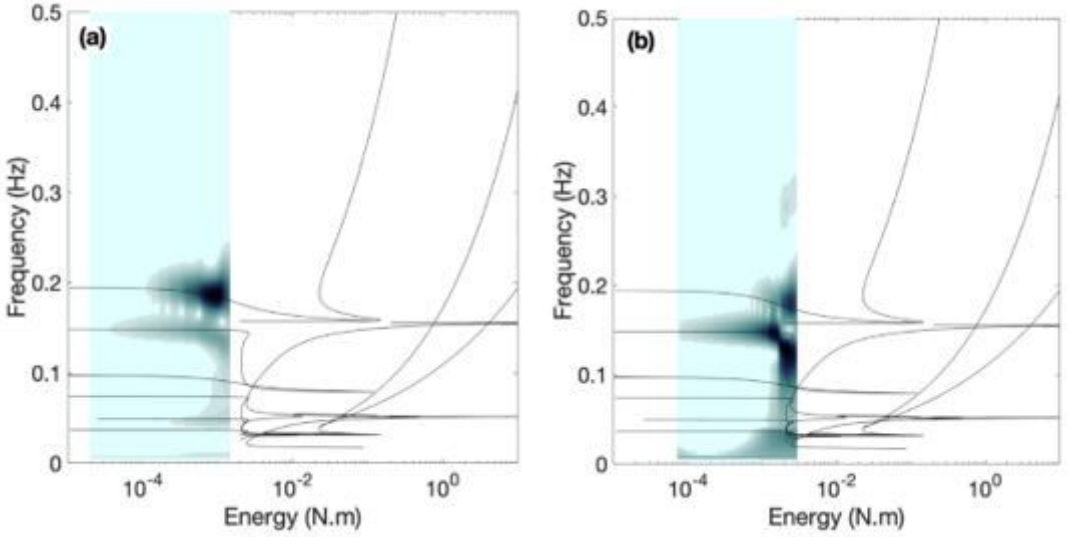

Figure 12

Caption for figure 12 can be found in the manuscript file.

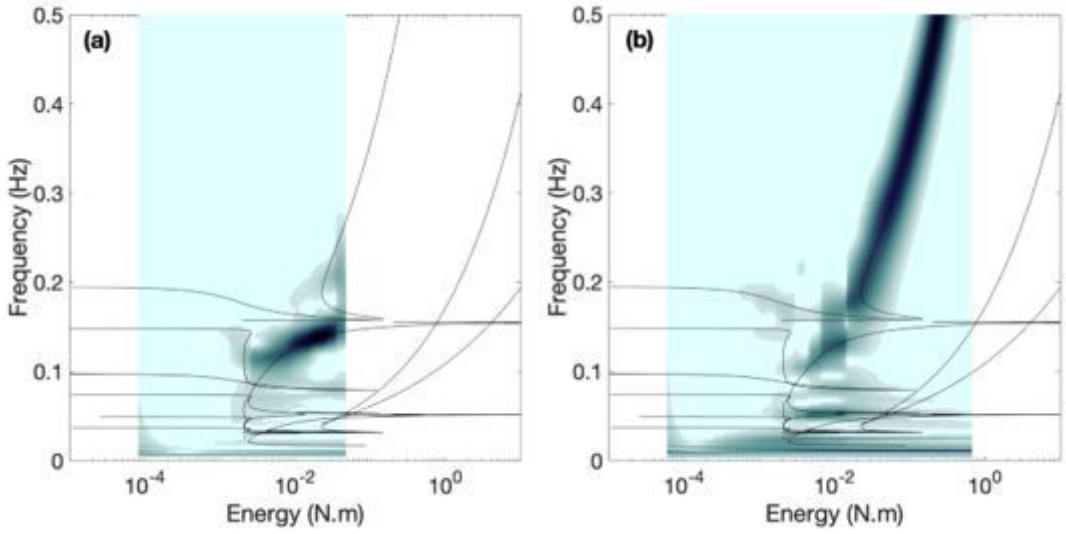

Figure 13

Caption for figure 13 can be found in the manuscript file.